NTNU
Det skapende universitet

Control of Thruster Assisted Position Mooring System on Floating Production Storage and Offloading

Helle Kristine H Olafsen

Marin teknikk
Innlevert: juni 2014
Hovedveileder: Asgeir Johan Sørensen, IMT

Norges teknisk-naturvitenskapelige universitet
Institutt for marin teknikk

NTNU Trondheim
Norwegian University of Science and Technology
Department of Marine Technology

MASTER THESIS IN MARINE CYBERNETICS

SPRING 2014

FOR

STUD. TECH. Helle Kristine Hovstad Olafsen

Design, Modeling and Control of Floating Production Storage and Offloading (FPSO) Unit with Thruster Assisted Mooring

Work description

In order to meet the world's growing energy demands, oil production is forced to move into deeper waters and harsher environments. Purpose-built Floating Production Storage and Offloading (FPSO) units have therefore become more common. For fields with several critical environmental load directions, a turret mooring configuration allows for weather waning, which minimizes vessel motion.

Thruster assisted position mooring systems (POSMOOR or TAMS) allows for larger operating windows, and increased safety in extreme conditions, both for spread- and turret moored vessels. The mooring system decreases the level of thrust needed, while the thrusters increase position keeping precision and weather waning capabilities.

Choice of mooring configuration is highly dependent on environmental conditions at the installation site, and should be robust enough to keep position even in the case of failure in the thruster system. A mooring system will be suggested and modeled. Control of the thruster system will then be investigated, and control objective formulated, with the purpose of reducing slow resonant motions and obtain stability in thruster assisted position mooring. The simulations will be conducted in Matlab/Simulink during the spring of 2014.

Scope of work

- Review relevant literature on thruster assisted position mooring
- Describe the various mooring- and turret configurations and design a system based on defined requirements
- Formulate both kinematic and kinetic models of the vessel dynamics and implement into Matlab/Simulink
- Implement an observer for wave and noise filtering
- Develop algorithms for detection of mooring line breakage and loss of mooring line buoyancy elements (MLBEs), and implement in the model
- Purpose control objectives and develop control algorithms and controllers
- Document each step in the process

The report shall be written in English and edited as a research report including literature survey, description of mathematical models, description of control algorithms, simulation results, discussion and a conclusion including a proposal for further work. Source code should be provided on a CD with code listing enclosed in appendix. It is supposed that Department of Marine Technology, NTNU, can use the results freely in its research work, unless otherwise agreed upon, by referring to the student's work. The thesis should be submitted in two copies within june 10th.

Advisers:Associated prof. II Anne Marthine Rustad

Professor Asgeir J. Sørensen
Supervisor

Abstract

This thesis is a study on mooring systems on floating production storage and offloading (FPSO) units, and includes the description of as well as a model containing a thruster assisted position mooring (POSMOOR) system. The main focus on the thesis was to get a better understanding of the different systems that are needed to perform position mooring.

A discussion on what sort of mooring system to is presented in the introduction, followed by an example of a turret moored unit. A six degree of freedom model has been described and implemented in Matlab/Simulink, using parameters provided by the Marine Cybernetics Lab, on the Cybership III. Some of these parameters are rough estimates or very uncertain, and may be updated during later work.

The mooring line dynamics have been described using the finite element method, based on the work done by Ole Morten Aamo on the ABB Integrated Vessel Simulator, and integrated in the Simulink model.

Simulations have been run to ensure that the mooring line dynamics are described properly, and to investigate the weather waning capability without control.

Control objective has been determined, followed by a control plant model. Based on this a Nonlinear Passive Observer was tuned for wave filtering of the motions calculated by motion RAO table lookups. Decay tests were run to find the mooring systems total stiffness and damping. The control adapts as the weather conditions becomes bad through setpoint generation. A reference model was implemented as well for smooth reference trajectories between setpoints. PID controll was implemented and tuned.

Acknowledgments

This master thesis concludes the authors studies at Norwegian University of Science and Technology, and contains a lot of different aspects to both structural, hydrodynamic and control system modelling. I feel like I have been able to use a lot of things that I have learned during my studies. Fault tolerant control was intended, but unfortiunately I was not able to find the reason for the noisy measurements from the line tensions, before it was too late. However, a complete functioning POSMOOR system for normal operation has been studied. Through the work, I have gained deeper knowledge about position mooring systems, and in addition gained further experience in computer software, namely Matlab/Simulink. LaTeXhas also been used to write the report.

I would like to give a very special thanks to the team at the subsea division of BW Offshore for giving me the chance to learn about and work with mooring systems on FPSOs. My supervisor, Asgeir Sørensen and co-supervisor Anne Marthine Rustad had a lot of ideas and inspired me greatly. Thanks to their help I was able to broaden my perspective and apply my knowledge on both fields. I wish also to thank Ole Morten Aamo for allowing me to make use of his model of mooring lines.

Finally I would like to thank my parents and Kristoffer for all their support.

Helle Kristine Hovstad Olafsen
Trondheim, June 10, 2014

Abbreviations and Symbols

APL	Advanced production loading
COT	Center of turret
CS3	Cybership III
DNV	Det Norske Veritas
DOF	Degrees of freedom
DP	Dynamic positioning
FPSO	Floating production storage and offloading
FEM	Finite element method
LCS	Lower chain segment
LWS	Lower wire segment
MLBE	Mooring line buoyancy element
POSMOOR (PM)	Position mooring
PDE	Partial differential equation
RTM	Riser turret mooring
STL	Submerged turret loading
STP	Submerged turret production
UCS	Upper chain segment
UWS	Upper wire segment
VLA	Vertically loaded anchors

β_c	Current angle of attack
γ_{rw}	Wind angle of attack
$\boldsymbol{\eta}$	Position and orientation vector in Earth-fixed frame
θ	Pitch angle
$\boldsymbol{\nu}$	Translational and rotational velocity vector
$\boldsymbol{\nu}_c$	Current velocity vector
$\boldsymbol{\nu}_r$	Relative velocity
ρ	Density of seawater
ρ_0	Mass per unit length
ρ_a	Air density
ρ_m	Mooring line density
ρ_w	Seawater density
$\boldsymbol{\tau}_{1wave}$	First order wave excitation vector
$\boldsymbol{\tau}_{2wave}$	Vector of second order wave loads
$\boldsymbol{\tau}_H$	Vector of hydrodynamic forces and moments
$\boldsymbol{\tau}_{RB}$	Vector of generalized forces and moments for the rigid body
$\boldsymbol{\tau}_{thrust}$	Vector of generalized control forces and moments
$\boldsymbol{\tau}_{wind}$	Vector of forces and moments associated with wind

ϕ	Hang-off angle
ϕ	Roll angle
ψ	Yaw angle (heading)
ψ_d	Desired heading
$\mathbf{a}$	Acceleration
A	Sectional area of mooring line
A_0	Cross-sectional area in unstretched condition of mooring line
A_{Fw}	Projected wind-area in surge
A_{Lw}	Projected wind-area in sway
C_A	Added mass coefficient
$\mathbf{C}_A$	Added Coriolis and centripetal matrix
C_{DN}	Normal drag coefficient
C_{DT}	Tangential drag coefficient
C_K	Wind coefficient in roll
C_M	Wind coefficient in pitch
C_N	Wind coefficient in sway
$\mathbf{C}_{RB}$	Rigid body Coriolis and centripetal matrix
C_X	Wind coefficient in surge
C_Y	Wind coefficient in sway
C_Z	Wind coefficient in heave
d	Cable diameter
D	Nominal diameter
D	Down coordinate
$\mathbf{D}(\boldsymbol{\nu}_r)$	Collection of damping effects
$\mathbf{D}_p(\omega)$	Wave radiation damping matrix
e	Strain
E	Modulus of elasticity of mooring line material
E	East coordinate
$\mathbf{f}$	Sum of external forces
g	Acceleration of gravity
$\mathbf{G}$	Matrix of linearized restoring coefficients
$\mathbf{G}(\boldsymbol{\eta})$	Vector of restoring forces and moments
h	Water depth
H_{Fw}	Centroid of projected wind-area in surge
H_{Lw}	Centroid of projected wind-area in sway
H_s	Significant wave height
$\mathbf{J}(\boldsymbol{\eta})$	Rotation matrix
l	Segment length
L	Unstretched length of mooring line
L_{oa}	Length over all
l_s	Unstretched length of mooring line
m	Number of mooring lines
$\mathbf{M}$	Combined inertia and added mass matrix
$\mathbf{M}(\omega)$	Inertia matrix including frequency dependent added mass coefficients
$\mathbf{M}_A$	Added mass matrix
$\mathbf{M}_{RB}$	Rigid body mass matrix
n	Number of mooring line segments
N	North coordinate
p	Roll angular velocity
q	Pitch angular velocity
r	Yaw angular velocity
$\mathbf{r}$	Position vector

$\mathbf{R}(\psi)$	Rotation matrix (3-DOF)
s	Arbitrary point along the unstretched length of a mooring line
t	Time
$\mathbf{t}$	Tangential vector
T	Tension
T_H	Horizontal component of top tension
T_p	Peak period
T_z	Vertical component of top tension
u	Surge velocity
$\mathbf{u}$	Control input vector
v	Sway velocity
$\mathbf{v}$	Velocity
V_c	Current speed
V_{rw}	Relative wind-speed
w	Heave velocity
w	Submerged weight per unit length of mooring line
x	Horizontal distance from hang-off to touch-down point
X	Body-fixed reference frame, x-coordinate
x_d	Desired x-position
X_E	Earth-fixed reference frame, x-coordinate
X_R	Reference parallel frame, x-coordinate
Y	Body-fixed reference frame, y-coordinate
y_d	Desired y-position
Y_E	Earth-fixed reference frame, y-coordinate
Y_R	Reference parallel frame, y-coordinate
Z	Body-fixed reference frame, z-coordinate
Z_E	Earth-fixed reference frame, z-coordinate
Z_R	Reference parallel frame, z-coordinate

Contents

Chapter 1

Introduction

1.1 Motivation

Due to the trend of oil production moving towards remote and deep water locations, FPSO (Floating Production Storage and Offloading) units are increasingly used in the oil and gas industry. Safety is a primary concern on an FPSO, as the oil recovery process is high risk. In order to move into deeper waters and harsher conditions, strict requirements have to be met to ensure crew safety and reduce risk of damaging the environment. The operations may have to be halted if weather conditions exceeds the limit for which the unit is designed, which results in great production losses.

1.2 Previous Work

For all FPSO contractors, whenever there is a new project, decisions has as to what sort of mooring system to equip the vessel with, as this will have great impact on the investment and production costs, the safety on board, and the weather restrictions. Mooring engineers such as Howell et al. (2006), has shared their experiences on the subject.

In order to adapt to the challenging environment in newer fields, such as in the arctic. By equipping the FPSO with a thrusted assisted position mooring system (POSMOOR), the operational weather windows can be extended to extreme weathers and risk of mooring line breakage kan be reduced, The modeling of a POSMOOR system differs from that of a DP system because of the influence of the mooring system on the vessel motions.

The application of position mooring systems has been explored since the 1980s, and has successfully been applied several times. FPSO units equipped with it can be found all over the world. Modeling At the Marine Cybernetics lab operated by the Department of Marine Technology, different model experiments using position mooring applied to Cybership III has earlier been conducted. Examples of earlier work in modeling and control of thruster assisted turret-moored ships can be found for instance in Strand et al. (1998) and Sørensen et al. (1999). Berntsen (2008) and Barth Berntsen et al. (2008) are more specific about the application of structural reliability based control in position mooring.

1.3 Contributions

This thesis is based on the modelling and design of a POSMOOR system for the full scale version of CSIII in deep water, with a flexibility to working conditions in moderate to extreme weather conditions.

A mooring configuration defined for deep water application of the full-scale CSIII vessel has been provided in **Chapter 3**. This is also the configurations used in the simulink model. Dimensioning of mooring line components has been done, and the physical parameters of the proposed system is also presented. The dynamics and kinematic behavour necessary to derive the process plant model is presented in **Chapter 4**. The FEM applied to mooring lines has also been descriped along with the elastic catenary.

The control system components are described in **Chapter 5**, and has been tuned according to the control objectives which are also stated here. The resulting simulink model contains an observer for wave filtering, and a reference model for smooth trajectory generation between the moderate and extreme SPs.

1.4 Organization of the Thesis

Chapter 2 describes the outline of mooring systems on FPSOs. A discussion on what needs to be considered when determining what sort of mooring system to use is also presented.

Chapter 3 contains a presentation of the turret mooring system that has been considered in the further work. Specifications on the different mooring components are given, and the physical simplifications of the system prior to the mathematical modeling are presented and argumented for.

Chapter 4 presents the mathematical modeling of a turret moored mooring system. The vessel dynamics are modeled and explained, in terms of kinetics and kinematics, low-frequency and wave-frequency motions. The catenary equations and finite element method that are applied on mooring lines are also explained.

Chapter 5 forms the basis on the implementation of a controller, and explains the control objective of a position mooring system. A control plant model based on the control objective is presented, followed by a short note on other control modes that may be relevant to the system. The description of the observer, reference model and kontroller can also be found here.

Chapter 6 contains the results from simulations done in Simulink, showing the dynamic behavior of the mooring lines and the vessel, and confirms its weather waning ability.

Chapter 7 forms the concluding chapter, in which the results are summarized and evaluated. Suggestions for possibilities for further work are also given here.

Appendix A Is a small Norwegian summary of the thesis.

Appendix B contains more data on the vessel, and its coefficients and system matrices.

Appendix C has a more comprehensive set of plots some of the simulations done in chapter 6

Appendix D contains the simulink block-diagrams.

Chapter 2

Mooring System Design

2.1 Mooring System

When designing the mooring system of an FPSO, several factors will need to be considered when determining what is the most efficient configuration. The configuration will greatly influence the other systems on the unit as well as the direct influence on investment and production costs as well as safety.

FPSOs are can either be moored to the seabed or dynamically positioned (DP). Full DP is the most accurate when it comes to seakeeping, but by far the most expensive to operate. Mooring solutions are therefore often preferred.

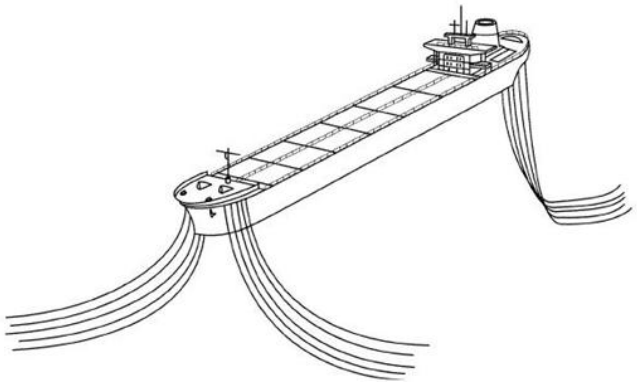

Figure 2.1: Spread moored FPSO (*Source: API*)

2.1.1 Spread Mooring

The mooring configuration can either be what is referred to as spread- or single point moored. A spread moored FPSO, illustrated in Figure 2.1, is a vessel moored by anchor legs from the bow and stern of the vessel in a four-group arrangement. With such an arrangement, the risers used for production and water injection, as well as the umbilicals are suspended from "riser porches"

on one of the vessel's sides. This mooring configuration causes a fixed orientation of the FPSO in global coordinates.

2.1.2 Turret Mooring

The most used kind of single point mooring system is the so-called turret solution. A turret moored FPSO allows the vessel to rotate around the turret connection point, while the mooring and turret itself is fixed. With such a configuration, the vessel can weather wane, which means it can align with the prevailing environmental direction. The turret provides the transfer of loads between the mooring and the vessel.

Weather waning reduces the total load on the ship, as well as the vessel wave frequency motions, and therefore significantly reduce the loads on the mooring system. In case of a turret mooring configuration, the risers and umbilicals are suspended from within the turret. As illustrated in

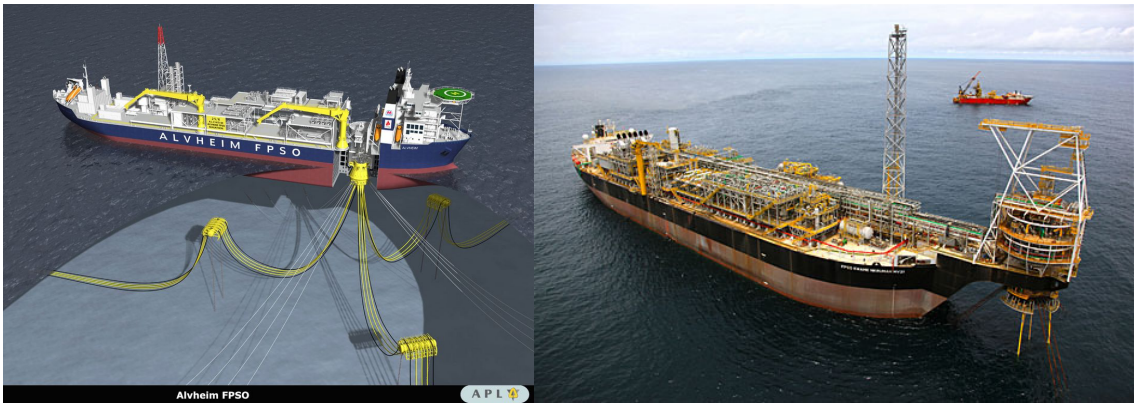

Figure 2.2: Internal and external turret moorings (*Source: APL and SOFEC*)

Figure 2.2, the turret can either be integrated within the ship's hull (internal) or as a part of an extended structure on the vessel bow (external). The external turret is especially applicable in shallow waters to increase distance to seabed and therefore facilitate the risers, as the chain connections are located above water level.

The external turret is cheaper than the internal turret solution, also when considering the amount of modification necessary on the vessel. However, integrating the turret yields higher structural reliability and better load-transfer characteristics (Wichers 2013).

In areas particularly exposed to extreme weather as hurricanes or typhoons, disconnectable turret solutions are used. When design weather criteria are exceeded, the vessel can disconnect, leaving a turret buoy at some designed depth beneath the water surface. By doing so, the risks are highly reduced, both for the structure and for the crew on board the vessel. A riser turret mooring (RTM) system, which involves a disconnectable external turret like in Figure 2.3, is such an alternative used for deepwater applications.

A submerged turret buoy solution is an integrated disconnectable turret solution, that is designed to stay at a certain design water depth in a disconnected state. The so-called submerged turret production (STP) solution is provided with a swiwel that deals with the transfer of fluid from the riser(s) to the production installation on the vessel. This is based on the technology of submerged turret loading (STL), with increased complexity when it comes to the swiwel.

Figure 2.3: Disconnectable turret (*Source: Navicom Dynamics*)

2.1.3 Thruster Assistance

By equipping a FPSO unit with a POSMOOR system, the thrusters assists the mooring, so that the FPSO can endure harsher weather, and even maintain production. Due to the thruster assistance, the resulting offset and motions are reduced, and the mooring lines are subject to less loads, reducing the probability of mooring line failure.

2.2 Choosing Mooring Configuration

When deciding what sort of mooring the planned FPSO is to be equipped with, there are a lot of factors to consider. Both spread and turret mooring can generally be applied, but the costs will vary greatly for different applications.

One apparent thought is that the fixed orientation of the spread mooring will make the system vulnerable to predominant weather coming from either of the ship's sides. The spread mooring is therefore best suited for areas largely dominated by a certain weather direction.

2.2.1 Mooring

Due to the load reduction provided by the weather waning capability of a turret mooring system, the mooring lines can in turn be fewer and/or less sturdy than that of a spread moored vessel for the same application. However, the turret itself, especially internal ones, can be quite expensive, depending on the number of risers and umbilicals necessary.

2.2.2 Risers and Umbilicals

An external turret is limited to only a few risers, while the most advanced and expensive internal turret systems these days can support more than 100 (Boatman et al. 2006). Spread moored units, on the other hand, have generally no restrictions for the riser balcony(-ies), and installation

cost doesn't increase as much with the number of risers.

The adding and other modifications of risers and umbilicals is not easily done with a turret mooring system. The turret must be planned and designed knowing the final number of risers at end of lifetime, and is therefore restricted compared with a riser balcony.

Another notable issue is that the risers have to be robust enough to withstand the motions that comes with the turret being placed at the vessel bow, where the motions are large.

2.2.3 Vessel Modifications

The internal turret performs better in terms of load transfer compared to the external turret, but comes with higher costs both due to the complexity of the turret itself and the modifications that needs to be done in order to fit it in the hull of the ship. The costs are so large that instead of modifying an existing vessel, newbuilds are becoming more and more common.

2.2.4 Seabed Arrangement

The mooring lines on a turret moored system can either be evenly distributed around the turret center, or arranged in groups, for example of three, as shown in Figure 2.4. The latter option adds flexibility in riser approaches. Since the seabed structures have to be arranged so that a possible torn mooring line will not fall on top of anything, this flexibility allows for more economical seabed arrangements. The seafloor area that can be utilized is also greater, as there are fewer anchor legs and/or anchor leg groups than for a spread moored vessel.

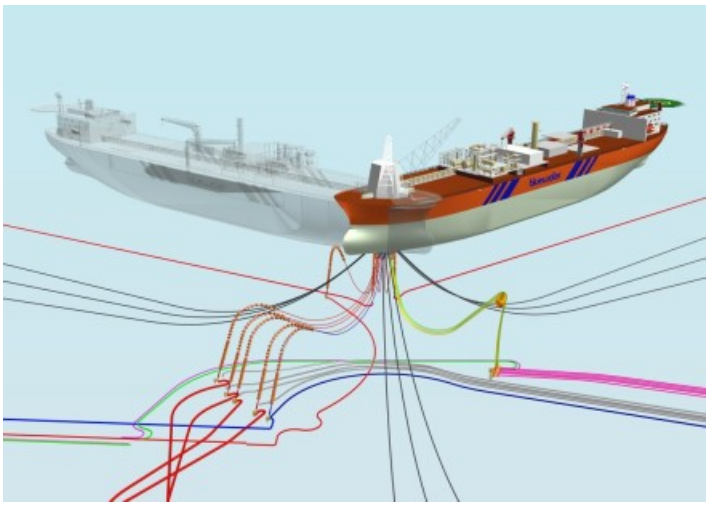

Figure 2.4: Mooring- and subsea arrangement (*Source: Bluewater*)

2.2.5 Installation

The risks associated with installation schedules can be reduced significantly with a disconnectable buoy-turret solution, because the installation of the mooring and riser system can be performed way before the hook-up of the FPSO. In many cases, the FPSO is on the critical line while

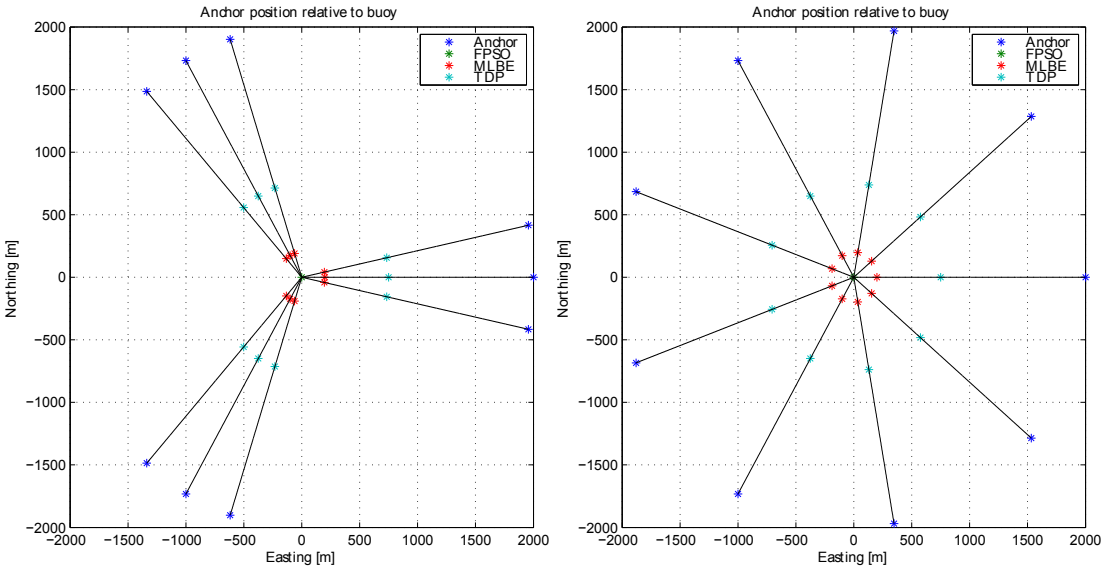

Figure 2.5: Mooring line arrangements

the mooring and riser system is not, which makes it attractive to install the subsea system well in advance of the arrival of the FPSO. The best installation window can be selected for the buoy, mooring and risers system, and it takes only a day to connect the vessel to the mooring. When the vessel is locked to the mooring system, the few remaining commissioning tasks can immediately be made on board the vessel.

2.2.6 Offloading

The fixed orientation of a spread moored FPSO, makes the offloading operation at high risk for collision with the offloading vessel. The risers hanging from the shipside are at risk to be damaged during side-by-side offloading, while the mooring lines grouped at the aft and bow are equally exposed during tandem offloading. Due to this, expensive satellite export systems may be considered.

With a turret moored configuration, this risk is eliminated, as the mooring and risers are concentrated. During offloading, both the FPSO and the shuttle tanker can align with the weather, which makes the approaching and offloading safer and more predictable.

Chapter 3

Mooring System Specification

For the simulations run in this assignment, a turret-moored FPSO in water depth of five hundred meters has been considered. This configuration was chosen, due to the flexibility of such a solution in terms of installation site.

3.1 Design Criteria

When determining the mooring system properties, such as the number of mooring lines, the material properties and so on, a number of class regulations and guidelines needs to be followed.

For mooring system analysis a combination employing both wind and waves with 100-year return periods together with current with a 10-year return period is usually considered (DNV).

Sea states with return periods of 100 years shall normally be used when designing position mooring systems (DNV). If the joint distribution of significant wave height (H_s) and peak periods (T_p) for the installation site is not available, then the range of combinations may be based on a contour line for the North Atlantic. Another option is to conduct a sensitivity analysis with respect to the peak period for the 100 year sea state.

3.2 Simulated Environment

Simulations were conducted in Simulink for a turret-moored vessel based on the physical properties of Cybership III (CS3), belonging to the Marine Cybernetics Lab.

For the simulations performed during this project, a preliminary choice of mooring system configuration has been used, as the calculations required to ensure that the mooring system satisfies the class requirements are too time consuming.

3.2.1 Waves

The sea state can be described using the significant wave height, H_s, which is the mean of the one-third largest waves, along with a characteristic period, such as the peak period T_p. When

wind travels the oceans, waves develop on the surface, and grow in size and period as the wind speed is maintained, until the sea state is fully developed. For developing sea, the *JONSWAP* spectrum is used, while if the seas are fully developed, the *Modified Pierson-Moskowitz* spectrum is recommended. In this assignment, only the JONSWAP spectrum will be investigated. The spectrum used is shown in Figure 3.1.

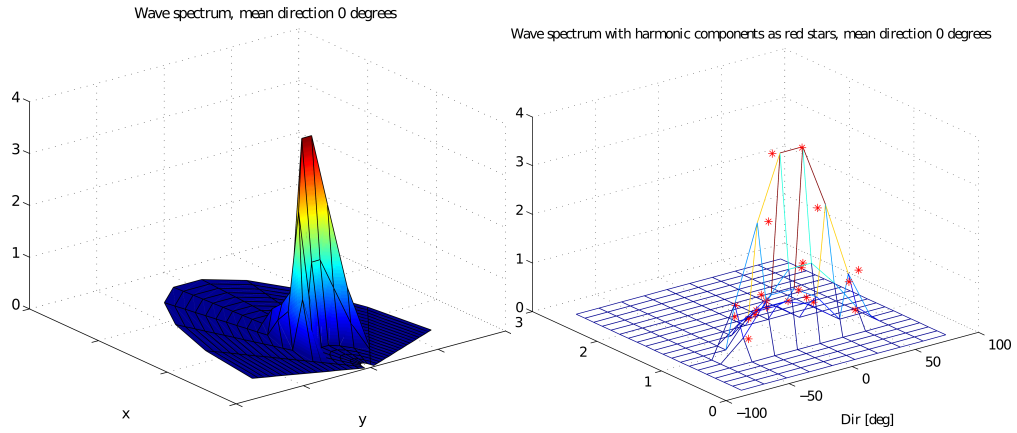

Figure 3.1: Jonswap spectrum, $H_s = 6$, $T_p = 7$

3.2.2 Wind

The wind force is calculated based on the wind coefficients given for CS3, which are plotted in Figure 3.2 (see section B.2 for the numbers). The wind coefficients in pitch and roll are estimated from the surge and sway coefficients. The wind has been considered time-invariant for the simulations in this work. The relationship between the wind velocity and the JONSWAP spectrum was found in Figure 8.8 in Fossen (2011), which for $H_s = 6$ gives a Beuford number of 7, which by definition is equivalent of a moderate gale and wind speeds of 14-17 m/s.

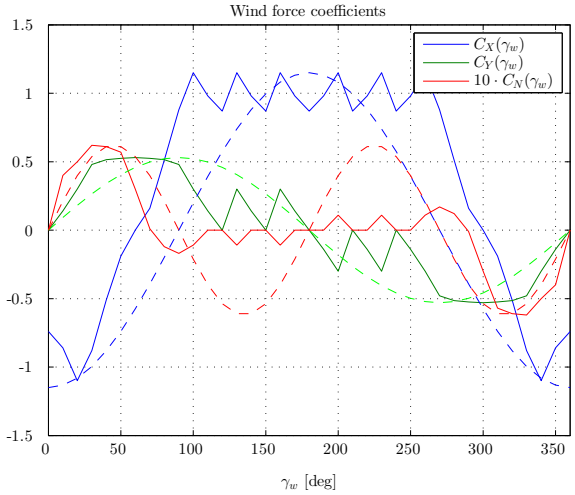

Figure 3.2: Wind coefficients in surge, sway and yaw

3.2.3 Current

The current is as described in chapter 4 represented in the state-space model as a forward speed. Current coefficients are also available for CS3 (section B.3), as an alternative way of accounting for it. It is, as the wind, assumed to be constant in this system. For it's effect on the mooring lines, it has been given a linear variation towards the seabed, with a factor of 0.8 at 200 meters depth. At the seafloor, the no-slip condition is used.

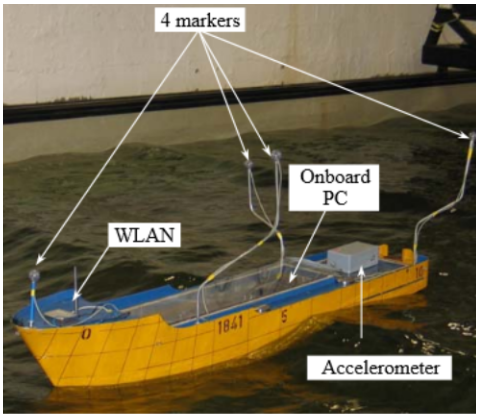

Figure 3.3: Cybership III (Dong 2006)

3.3 Vessel Data

The vessel used for the simulations is based on the full-scale version of Cybership III (CS3), shown in Figure 3.3, owned by the Marine Cybernetics Laboratory. The main properties of the model and the full-scale vessel are presented in Table 3.1.

Parameter	Unit	Model	Full Scale
Scale	[-]	1 : 30	-
Length between perpendiculars	[m]	1.971	59.13
Breadth	[m]	0.437	13.11
Draft	[m]	0.153	4.59
Displacement	[m^3]	0.075	2 025
Transverse metacentric height	[m]	0.02	0.60
Longship metacentric height	[m]	1.474	44.22
Waterplane area	[m^2]	0.656	590.4
Radius of gyration, roll	[m]	0.1713	5.139
Radius of gyration, pitch	[m]	0.5138	15.414
Radius of gyration, yaw	[m]	0.5138	15.414
Projected wind force area, surge (rough estimate)	[m^2]	0.0677	60.93
Projected wind force area, sway (rough estimate)	[m^2]	0.4	360
Projected current force area, surge	[m^2]	0.0620	55.8
Projected current force area, sway	[m^2]	0.25	225

Table 3.1: Vessel data for cybership III

3.3.1 Model scaling

The data for CS3 is only available for the model-size vessel. In order to perform simulation of a full scale vessel, the different data need to be scaled while ensuring (Steen 2013):

- **Geometrical Similarity:** The model and full scale structures must have the same shape
- **Kinematic Similarity:** The flow and model(s) must have geometrically similar motions in model and full scale
- **Dynamic Similarity:** Ratios between different forces in full scale must be the same in model scale

To help with this, a number of dimensionless numbers are used.

$$F_n = \frac{U}{\sqrt{gL}} \tag{3.1}$$

Equality in Froude number, Fn, which is given by the square of the ratio between inertia and gravity, yields dynamic similarity between model and full scale by ensuring that gravity forces are correctly scaled.

$$R_e = \frac{UL}{\nu} \tag{3.2}$$

The Reynolds number, Re, is the relationship between the inertia and viscous forces. Equality in Reynolds number will therefore ensure that the viscous effects are scaled correctly. The various

Physical parameter	**Unit**	**Scaling factor**
Length	[m]	λ
Structural mass	[kg]	$\lambda^3 \cdot \rho_f/\rho_m$
Force	[N]	$\lambda^3 \cdot \rho_f/\rho_m$
Moment	[Nm]	$\lambda^4 \cdot \rho_f/\rho_m$
Acceleration	[m/s^2]	1
Time	[s]	$\sqrt{\lambda}$
Pressure	[Pa]	$\lambda \cdot \rho_f/\rho_m$

Table 3.2: Froude scaling, $\lambda = L_f/L_m$

other data available for CS3 must also be scaled. This has been done using the parameter in question's SI-unit, and using the values in Table 3.2.

3.4 Seabed Layout

It is assumed that the seabed at the installation site is flat, and that the mooring lines may be evenly distributed around the turret, like illustrated in Figure 2.5, without any concern of a broken mooring line falling on top of equipment.

3.5 Mooring Lines

The mooring lines can either be made of chain, rope or a combination of both. Segmented mooring lines, having heavy chain at the bottom and a lighter line close to the surface, allows

for greater stiffness and lighter mooring lines (Faltinsen 1990).

Due to the water depth, the mooring lines needs to be equipped with mooring lines buoyancy elements (MLBEs) (*source: APL*), due to the restrictions on the turret in unhooked condition. Each mooring lines will therefore consist of the following segments (listed from anchor to hang-off, as illustrated in Figure 3.4)

- Lower chain segment (LCS) - on seafloor, connected to anchor
- Upper chain segment (UCS)
- Lower wire segment (LWS)
- Moorling line buoyancy elements with connections
- Upper wire segment (UWS) - with connection to turret

Generally the anchors are easily moved, and in order to avoid this, great lengths of chain along the seafloor are used (Faltinsen 1990). Depending on the seabed properties, the length can be shorter when the chain is submerged into the seabed (muddy soil), as this will reduce the slamming effects.

The upper chain segment is necessary since the wire part of the mooring lines is not allowed to touch the seafloor (DNV).

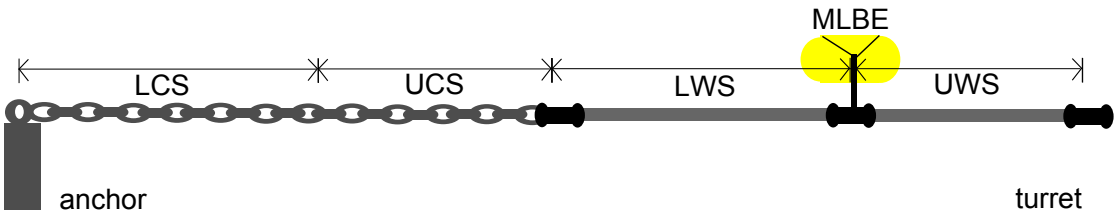

Figure 3.4: Mooring line systematic sketch

3.5.1 Chain

Chain have been given the quality of studless steel R4S chain, which is a high quality studless chain used for permanent offshore mooring systems. The properties are calculated by the formula given in Table 3.4, that are based on approximations used in the mooring line setup wizard for the mooring analysis program Orcaflex.

Property	**Studless chain**
Outer diameter	$1.80 \cdot D$
Inner diameter	0
Mass/Length	$19.9 \cdot D^2$
Axial Stiffness	$0.854 \cdot 10^8 \cdot D^2$
Bend Stiffness	0
Normal drag coefficient	1.0
Axial drag coefficient	0.4

Table 3.3: Chain properties (with nominal diameter D)

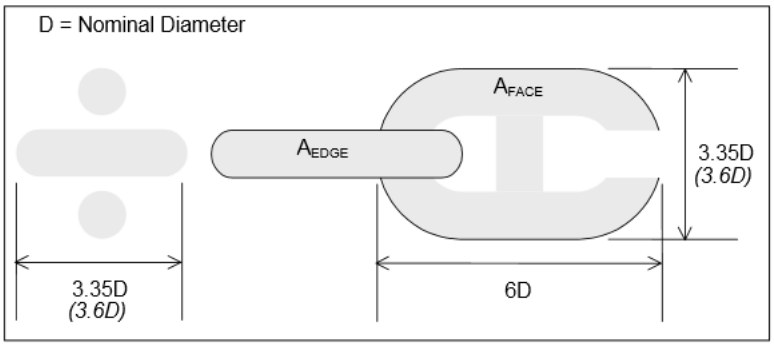

Figure 3.5: Chain geometry *(source: Ocarina)*

3.5.2 Wire rope

Wire with wire core has been implemented on the UWS and LWS parts of the mooring line. The corresponding physical properties can be found in Table 3.4.

Property	**Wire rope**
Outer diameter	$0.80 \cdot D$
Inner diameter	0
Mass/Length	$3.9897 \cdot D^2$
Modulus of elasticity	$1.13 \cdot 10^8 \cdot$
Metal covered area	$0.455\pi D^2/4$
Bend Stiffness	0
Normal drag coefficient	1.0
Axial drag coefficient	0.4

Table 3.4: Wire properties (with nominal diameter D)

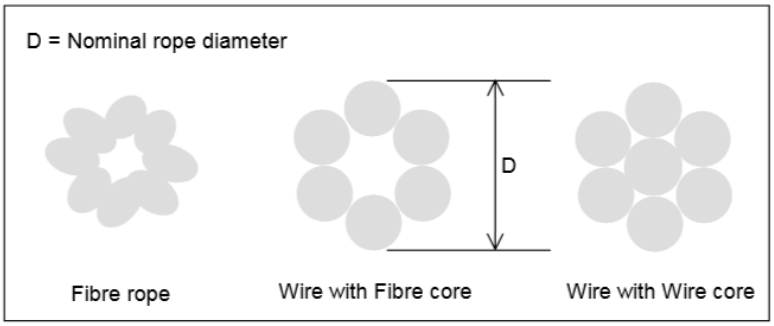

Figure 3.6: Wire geometry *(source: Ocarina)*

3.5.3 Mooring Line Buoyancy Elements

In deeper waters MLBEs are used to give a better horizontal restoring characteristic of the mooring system, without introducing excessive vertical forces from the mooring lines to the turret. The elements carry some of the weight of the long mooring lines, which for the STP

buoy solutions means that the net buoyancy of the buoy itself can be kept on a reasonable level (Aanesland et al. 2007). Such elements have a depth-restriction of about 200-300 meters (APL).

3.5.4 Anchors

Four types of anchors are used in mooring of FPSO's, namely pile-, torpedo-, suction- and drag anchors.

The anchor choice mainly influence the calculations in that some allows for more accurate installation than others, which means that the calculations might have to be redone with the updated anchor positions. Additionally, conventional anchors are restricted to only resisting horizontal loads. Traditionally most designers opt for the use of suctions piles, although in recent years a number of floating production units have been moored using vertically loaded anchors (VLAs).

By introducing long chain segments along the seabed, the loads on the anchor can be significantly reduced, especially when the seabed is soft so that the anchor segment becomes submerged into the seabed.

3.5.5 Assembly

Calculations have been run in Matlab, using the elastic catenary equations, to adjust the segment lengths to ensure that the touchdown point is located around the transition from the LCS to the UCS, and that the MLBE's are located at about 200 m depth.

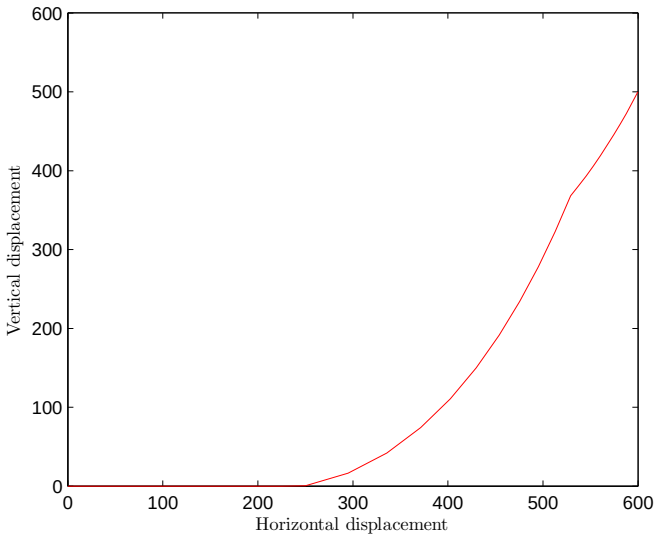

Figure 3.7: Mooring line profile

The segment lengths that yielded the most satisfying results in terms of shape and convergence of the method are given in Table 3.5

Segment	**LCS + UCS**	**LWS**	**UWS**
Length $[m]$	250	480	150
Nominal diameter $[m]$	0.09	0.024	0.024
Density $[kg/m^3]$	7820.2	7937.3	7937.3
Axial Stiffness $[N/m]$	3.4608e+07	5.112e+07	5.112e+07
MLBE $[kg]$	0	0	-8000
Finite elements	10	10	10
Normal drag coeff. $[-]$	1	1	1
Tangential drag coeff. $[-]$	0.5	0.5	0.5
Added mass coeff. $[-]$	1.5	1.5	1.5

Table 3.5: Mooring line properties

Chapter 4

Mathematical Modelling

4.1 Degrees of Freedom and Motions

The motions of a floating structure are divided into wave-frequency motion, high-frequency motion, slow-drift motion and mean drift (Faltinsen 1990). 6 degrees of freedom (DOF) are used to specify completely the displaced position and orientation of a marine craft (Fossen 2011). The motions along the translatory DOFs are referred to as *surge*, *sway* and *heave*, while the angular as *roll*, *pitch* and *yaw* (see Figure 4.1).

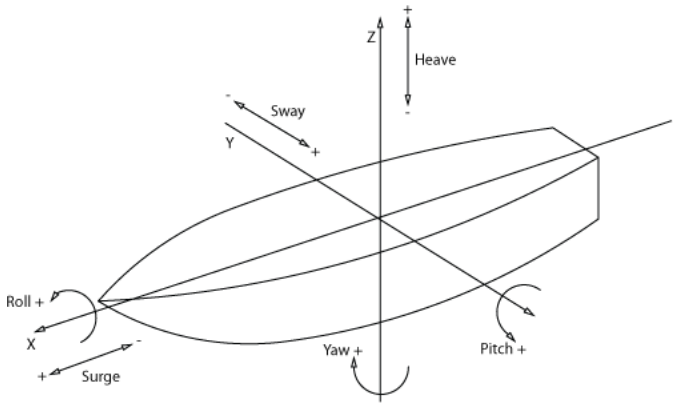

Figure 4.1: Definition of rigid-body motion modes

4.2 Kinematics

The reference frames used in the modeling are shown in Figure 4.2. The Earth-fixed reference frame, $X_E Y_E Z_E$, is placed at the mean water surface, with Z pointing downwards. The Body-fixed reference frame, XYZ, is placed at the mean position of the center of gravity, with the X-axis going from aft to fore, the Y-axis going to the starboard, and the Z-axis downwards.

The position and orientation of the vessel in the Earth-fixed reference frame are denoted $\boldsymbol{\eta} = [N\ E\ D\ \phi\ \theta\ \psi]^T$ (Fossen 2011). $\boldsymbol{\nu} = [u\ v\ w\ p\ q\ r]^T$ is the translational and rotational

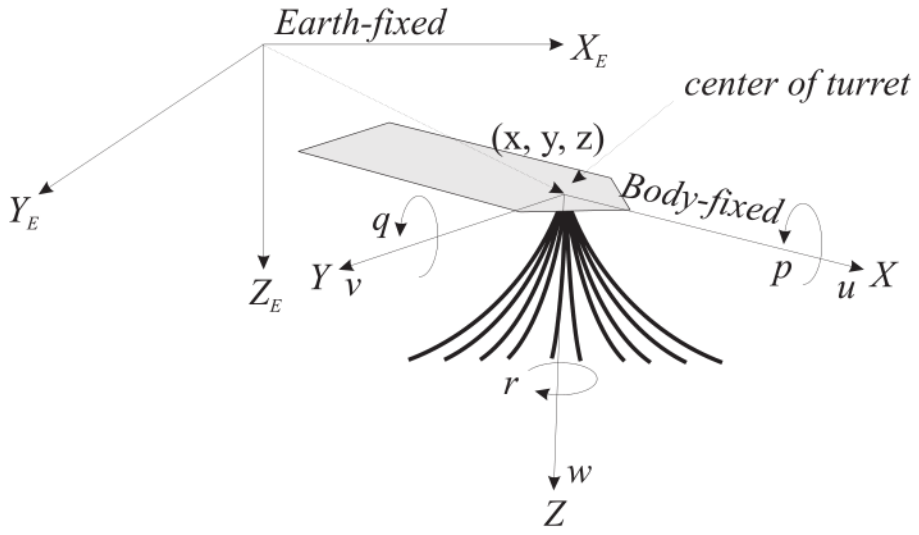

Figure 4.2: Reference frames

velocities in the body-fixed frame as seen in Figure 4.3. The two are related by the rotation matrix, $\mathbf{J}(\boldsymbol{\eta})$, so that

$$\dot{\boldsymbol{\eta}} = \mathbf{J}(\boldsymbol{\eta})\boldsymbol{\nu} \tag{4.1}$$

The transformations can be found in Fossen (2011), resulting in the following relationship ($s = \sin,\ c = \cos,\ t = \tan$)

$$\mathbf{J}(\boldsymbol{\eta}) = \begin{bmatrix} \mathbf{J}_1(\boldsymbol{\eta}) & \mathbf{0} \\ \mathbf{0} & \mathbf{J}_2(\boldsymbol{\eta}) \end{bmatrix}$$

$$\mathbf{J}_1(\boldsymbol{\eta}) = \begin{bmatrix} c\psi c\theta & -s\psi c\theta + c\psi s\theta s\phi & s\psi s\phi + c\psi c\phi s\theta \\ s\psi c\theta & c\psi c\phi + s\phi s\theta s\psi & -c\psi s\phi + s\theta s\psi c\phi \\ -s\theta & c\theta s\phi & c\theta c\phi \end{bmatrix}$$

$$\mathbf{J}_2(\boldsymbol{\eta}) = \begin{bmatrix} 1 & s\phi t\theta & c\phi t\theta \\ 0 & c\phi & -s\phi \\ 0 & s\phi/c\theta & c\phi/c\theta \end{bmatrix}$$

For a models only considering motions in surge, sway and yaw, (4.1) is reduced to (Fossen 2011)

$$\dot{\boldsymbol{\eta}} = \mathbf{R}(\psi)\boldsymbol{\nu} \tag{4.2}$$

where

$$\mathbf{R}(\psi) = \begin{bmatrix} \cos(\psi) & -\sin(\psi) & 0 \\ \sin(\psi) & \cos(\psi) & 0 \\ 0 & 0 & 1 \end{bmatrix} \qquad \boldsymbol{\eta} = \begin{bmatrix} N & E & \psi \end{bmatrix} \qquad \boldsymbol{\nu} = \begin{bmatrix} u & v & r \end{bmatrix} \tag{4.3}$$

4.2.1 Transformations between COH and COT

The modelling in this chapter is based on the equation of motion for a free floating body. These are usually defined in the hydrodynamic center of the vessel (COH), as this is where the

rotational degrees of freedom will rotate about. For a point-moored system, it is convenient to transform the equations of motion to the center of turret (COT). The transformation of the motion to an arbitrary point, p, on the body, is described by Fossen (2011) using a transformation matrix, $\mathbf{H}(\mathbf{r}_p^b)$, which defines the relationship between the velocities in the two frames. From the equations described in the next part of this chapter, the resulting transformations are as follows:

$$\begin{aligned}
\boldsymbol{\tau} &= \mathbf{H}^T(\mathbf{r}_p^b)\boldsymbol{\tau}_p \\
\Rightarrow \mathbf{M}_p &= \mathbf{H}^{-T}(\mathbf{r}_p^b)\mathbf{M}\mathbf{H}^{-1}(\mathbf{r}_p^b) \\
\mathbf{C}_p(\boldsymbol{\nu}) &= \mathbf{H}^{-T}(\mathbf{r}_p^b)\mathbf{C}(\boldsymbol{\nu})\mathbf{H}^{-1}(\mathbf{r}_p^b) \\
\mathbf{D}_p(\boldsymbol{\eta}) &= \mathbf{H}^{-T}(\mathbf{r}_p^b)\mathbf{D}(\boldsymbol{\eta})\mathbf{H}^{-1}(\mathbf{r}_p^b) \\
\mathbf{g}_p &= \mathbf{H}^{-T}(\mathbf{r}_p^b)\mathbf{g}(\boldsymbol{\nu})
\end{aligned}$$

Where $\mathbf{r}_p^b$ is the vector from the body-fixed reference frame to the point. This is the same procedure that has been implemented on the vessel parameters that were defined in other reference frames.

4.3 Vessel Motions

The modeling for marine vessels is a complicated and highly nonlinear system. For a model-based observer and controller design, a simplified mathematical model of the vessel dynamics will suffice. In order to test the performance of the system, a more accurate description is needed. The modeling of the system may therefore be divided into two accuracy levels (Sørensen 2013), namely a *control plant model* and a *process plant model*. However, the process plant model can also be simplified to different cases depending on the control objectives, constraints and dynamic behavior of the system. For instance, the model is commonly simplified to consider the motions in surge, sway and yaw only. In the following, a process plant model of a moored vessel will be described in all 6-DOF.

Rigid Body Dynamics

The equations of motion in 6 DOF of a rigid body is given by (Fossen 2011)

$$\mathbf{M}_{RB}\dot{\boldsymbol{\nu}} + \mathbf{C}_{RB}(\boldsymbol{\nu})\boldsymbol{\nu} = \boldsymbol{\tau}_{RB} \tag{4.4}$$

Where $\mathbf{M}_{RB}$ is the inertia matrix, $\mathbf{C}_{RB}$ is the Coriolis and sentripetal matrix, and $\boldsymbol{\tau}_{RB}$ is the generalized external forces and moments for the rigid body.

Hydrodynamic Effects

For a rigid body moving in water, in addition to control- and environmental forces, a number of hydrodynamic effects, referred to as $\boldsymbol{\tau}_H$, will need to be considered.

$$\boldsymbol{\tau}_{RB} = \boldsymbol{\tau}_{thrust} + \boldsymbol{\tau}_{wind} + \boldsymbol{\tau}_{waves} + \boldsymbol{\tau}_{hs} + \boldsymbol{\tau}_H \tag{4.5}$$

The hydrostatic forces, $\boldsymbol{\tau}_{hs} = \mathbf{0}$ in the horizontal plane (Fossen 2011).

The effects of current and wind are calculated from a velocity, $\boldsymbol{\nu}_r$, relative to the vessel velocity. Given the kinematic relationship in (4.1), for a current of velocity V_c coming from β_c

$$\boldsymbol{\nu}_r = \boldsymbol{\nu} - \boldsymbol{\nu}_c = \begin{bmatrix} u \\ v \\ w \\ p \\ q \\ r \end{bmatrix} - \mathbf{J}^{-1}(\boldsymbol{\eta}) \begin{bmatrix} V_c \cos\beta_c \\ V_c \sin\beta_c \\ 0 \\ 0 \\ 0 \\ 0 \end{bmatrix}$$

where $\boldsymbol{\nu}_c$ is the current velocity, given in the body fixed frame. For direction conventions on the environmental loads, see Figure 4.3. The hydrodynamic effects can then be found according to Fossen (2011)

$$\boldsymbol{\tau}_H = -\mathbf{M}_A\dot{\boldsymbol{\nu}}_r - \mathbf{C}_A(\boldsymbol{\nu}_r)\boldsymbol{\nu}_r - \mathbf{D}(\boldsymbol{\nu}_r) - \mathbf{G}(\boldsymbol{\eta}) \tag{4.6}$$

Where $\mathbf{M}_A$ is the added mass matrix, $\mathbf{C}_A$ is the added Coriolis and centripetal matrix, $\mathbf{G}(\boldsymbol{\eta})$ are the restoring forces, and $\mathbf{D}(\boldsymbol{\nu}_r)$ represents the damping effects such as radiation, skin friction, wave drift and vortex-shedding.

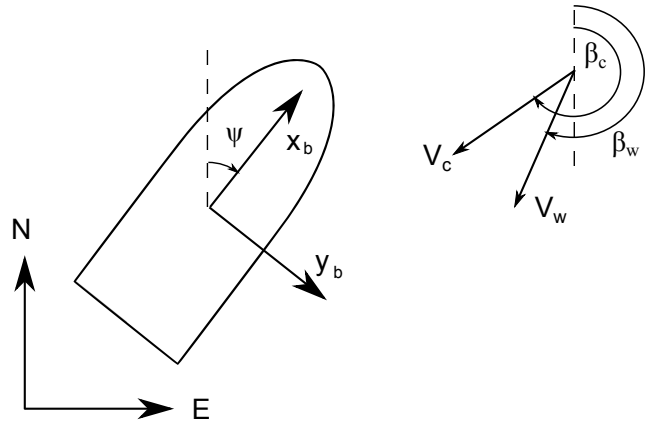

Figure 4.3: Directions of environmental loads

Wind

Given area-based wind-coefficients, the resulting force is, according to Fossen (2011)

$$\boldsymbol{\tau}_{wind} = \frac{1}{2}\rho_a V_{rw}^2 \begin{bmatrix} C_X(\gamma_{rw})A_{Fw} \\ C_Y(\gamma_{rw})A_{Lw} \\ C_Z(\gamma_{rw})A_{Fw} \\ C_K(\gamma_{rw})A_{Lw}H_{Lw} \\ C_M(\gamma_{rw})A_{Fw}H_{Fw} \\ C_N(\gamma_{rw})A_{Lw}L_{oa} \end{bmatrix} \tag{4.7}$$

Where $V_{rw} = \sqrt{(u-u_w)^2 + (v-v_w)^2}$ and $\gamma_{rw} = -atan2((v-v_w),(u-u_w))$ are the relative wind-speed with corresponding angle of attack, respectively. The projected wind-areas in surge and sway are A_{Fw} and A_{Lw}, with corresponding centroids H_{Fw} and H_{Lw}.

4.3.1 Low-frequency Motion Model

Position moored (PM) vessels can be regarded as a *stationkeeping* or low velocity application (Sørensen 2013). For convenience, the modelling is separated between low frequency (LF) and wave frequency (WF) motions, which can be superpositioned (Sørensen 2013). As the names suggest, the first order wave loads are not included in the study of low-frequency motions. Equations (4.4), (4.5) and (4.6) are combined to yield

$$\begin{aligned}\mathbf{M}\dot{\boldsymbol{\nu}} + \mathbf{C}_{RB}(\boldsymbol{\nu})\boldsymbol{\nu} + \mathbf{C}_A(\boldsymbol{\nu}_r)\boldsymbol{\nu}_r + \mathbf{D}(\boldsymbol{\nu}_r) + \mathbf{G}(\boldsymbol{\eta}) = \\ \boldsymbol{\tau}_{thrust} + \boldsymbol{\tau}_{wind} + \boldsymbol{\tau}_{2wave} + \boldsymbol{\tau}_{mooring}\end{aligned} \tag{4.8}$$

Where $\mathbf{M}$ is the combined inertia and added mass matrix, assuming $\dot{\boldsymbol{\nu}}_r = \dot{\boldsymbol{\nu}}$ for constant current. The second order wave loads $\boldsymbol{\tau}_{2wave}$ include slowly varying (difference frequencies)- and wave drift loads. Rapidly varying (sum frequency) wave loads are of higher frequencies and does not need to be included for control applications (Sørensen 2013). The mooring system force $\tau_{mooring}$, has also been added to (4.5).

4.3.2 Wave-frequency Motion Model

The hydrodynamic problem in regular waves is dealt with in two parts, namely *wave excitation loads* and *wave reaction loads* (Faltinsen 1990). The wave exciting forces and moments on a structure are found by restraining the vessel from moving, while the wave reaction loads are found by forcing the structure to oscillate with the wave excitation frequency. The equations for the wave frequency motions are assumed to be linear, so that the two problems can be added by the principle of superposition. The results is given by Sørensen (2013)

$$\begin{aligned}\mathbf{M}(\omega)\ddot{\boldsymbol{\eta}}_{Rw} + \mathbf{D}_p(\omega)\dot{\boldsymbol{\eta}}_{Rw} + \mathbf{G}\boldsymbol{\eta}_{Rw} = \boldsymbol{\tau}_{1wave} \\ \dot{\boldsymbol{\eta}}_w = \mathbf{J}(\psi_d)\dot{\boldsymbol{\eta}}_{Rw}\end{aligned} \tag{4.9}$$

which for station keeping analysis is given in the reference parellel frame $X_R Y_R Z_R$ (Sørensen 2013), positioned in the desired position of the vessel (x_d, y_d) and rotated to the desired heading ψ_d. $\mathbf{M}(\omega)$ is the system inertia matrix including frequency dependent added mass coefficients. $\mathbf{D}_p(\omega)$ is the wave radiation damping matrix. $\mathbf{G}$ contains the linearized restoring coeffients and $\boldsymbol{\tau}_{1wave}$ is the first order wave excitation vector.

4.3.3 Wave response

The response of the vessel due to the waves can be found using *Force-* or *Motion Response Amplitude Operators* (RAOs) or linear state-space models (Fossen 2011). The motion RAOs for CS3, scaled with Froudes number ($\omega_{w,f} = \omega_{w,m}/\sqrt{\lambda}$) are given in section B.4

The force from Force RAOs is added to the generalized force, and must be applied in both the WF and the LF model to get both excitation and drift forces. The response calculated from Motion RAOs however, will account for both terms.

4.4 Mooring System

Usually, the restoring forces caused by the mooring system is calculated using simplified quasi-static formulations using catenary formulas. These formulations only consider the static

equilibrium for each mooring line at each time step. As mooring systems are operating in increasing water depth, effects due to the nonlinear dynamic behavior and the interaction between fluid and mooring line are becoming increasingly important. Therefore, the real mooring force might exceed the predicted forces obtained from simplified calculations considerably.

4.4.1 The Elastic Catenary

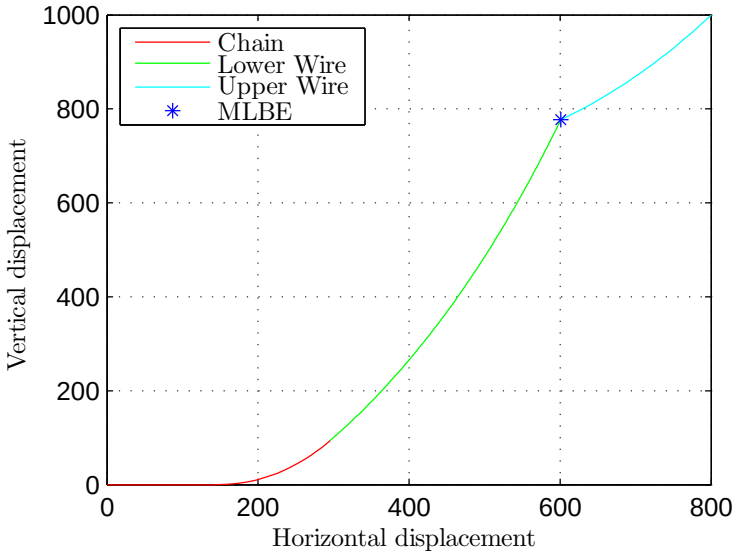

Figure 4.4: Catenary of a multi-segment mooring line

A typical catenary shape of a multi-segment mooring line is shown in Figure 4.4. The method is thoroughly described in Faltinsen (1990), but the main result is described here for reference.

To perform the calculations, a horizontal seabed is assumed and bending stiffness is neglected, which is a good approximation for chains and wires with large curvature (Faltinsen 1990). The static tension of an element along the cable can by examining Figure 4.5 for small $\alpha(x)$ and introducing hydrostatic pressure be expressed

$$dT - \rho g A dz = \left(w \sin\phi - F\left(1 + \frac{T}{AE}\right)\right) ds$$
$$T d\phi - \rho g z A d\phi = \left(w \cos\phi + D\left(1 + \frac{T}{AE}\right)\right) ds$$

The catenary equations are derived by neglecting the effects of the current, F and D, and elasticity introduced by including the relationship between the stretched length and unstretched length, ds, of an element

$$T - \rho g z A = T' \qquad \Rightarrow \begin{cases} dT' & = w \sin\phi ds \\ T' d\phi & = w \cos\phi ds \end{cases} \qquad \Rightarrow T' = T'_0 \frac{\cos\phi_0}{\cos\phi} \tag{4.10}$$

$$dp = ds(1 + \frac{T}{EA}) \tag{4.11}$$

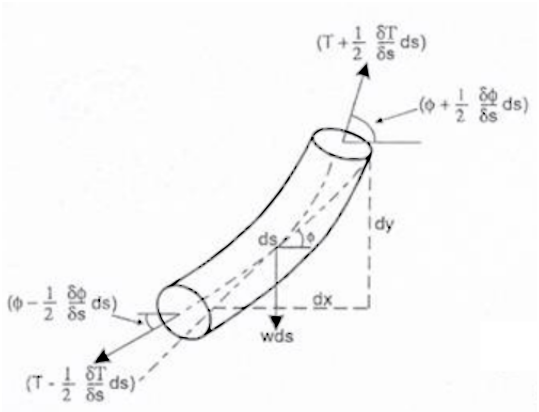

Figure 4.5: Catenary segment (*Source: Offshoremoorings.org*)

The top tension T is expressed by a vertical and a horizontal component, T_z and T_H, defined as (Faltinsen 1990)

$$T_z = l_s w \tag{4.12}$$

$$T_H = \frac{T_z^2 - \left(wh - \frac{1}{2}\frac{w^2}{EA}l_s^2\right)}{2\left(wh - \frac{1}{2}\frac{w^2}{EA}l_s^2\right)} \tag{4.13}$$

$$T = \sqrt{T_z^2 + T_H^2} \tag{4.14}$$

where l_s is the unstretched length of the cable from hang-off to touch-down point (TDP), w is the submerged weight of the cable, and h is the water depth. The horizontal distance from hang-off to TDP, x, can be found by

$$x = \frac{T_H}{w}\log\left(\frac{\sqrt{T_z^2 + T_H^2} + T_z}{T_H} + \frac{T_H}{EA}l_s\right) \tag{4.15}$$

The so-called *shooting method* has been used. The vertical tension, T_z and the hang-off angle, ϕ, of the mooring line is used to calculate the catenary shape by stepping through the segments from the top towards the TDP. The anchor position is then found by adding the rest of the mooring line, not included in l_s to x. If it does not match the prescribed anchor position, the tension and hang-off are updated. The calculations are repeated and the results interpolated until the anchor position is correct.

4.4.2 Finite Element Method on Mooring Lines

As investigated by several authors (for instance Aamo & Fossen (2001)), the dynamics of the mooring lines can be found using the *Finite element method* (FEM). The elastic catenary of the mooring lines can serve as an initial state for the iterations. However, if the current is large, the result from the elastic catenary may be too far away from the equilibrium to provide a good initial state for the iterations, as the current effects where neglected in (4.10). To avoid this problem, the current can be applied with increasing velocity divided by time steps. By choosing a small enough time interval, one can omit the Jacobian for the drag forces (Rustad 2013).

Bending and torsional stiffness may be included in the analysis, and therefore avoiding the

singularity that occurs for zero strain. For a mooring system, the lines are tensioned, and this is therefore not necessary to include in the model, as it may increase the calculation time drastically and perhaps unnecessarily.

Description of the Method

With the simplifications above, the motion of a point, $s \in [0, L]$, at the given time, $t \in [t_0, \infty]$, along the unstretched mooring line is given by (Aamo & Fossen 2001)

$$\rho_0 \frac{\delta \mathbf{v}(t,s)}{\delta t} = \frac{\delta}{\delta s}\left((T(t,s)\mathbf{t}(t,s)) + \mathbf{f}(t,s)(1+e(t,s))\right) \tag{4.16}$$

where
L: unstretched length of mooring line
ρ_0: mass per unit length
T: tension
e: strain
$\mathbf{v}$: velocity
$\mathbf{t}$: tangential vector
$\mathbf{f}$: sum of external forces

Expressing this in terms of a position vector, $\mathbf{r}$, and applying Hooke's law, (4.16) becomes

$$\rho_0 \frac{\delta^2 \mathbf{r}}{\delta t^2} = \frac{\delta}{\delta s}\left(EA_0 \frac{e}{1+e}\frac{\delta \mathbf{r}}{\delta s}\right) + \mathbf{f}(1+e) \tag{4.17}$$

The external forces includes gravitational and buoyancy forces, hydrodynamic forces (trangential and normal drag) and the hydrodynamic added mass, given by (Aamo & Fossen 2001):

$$\begin{aligned}
\mathbf{f}_{hg} &= \rho_0 \frac{\rho_m - \rho_w}{(1+e)\rho_m} \\
\mathbf{f}_{dt} &= -\frac{1}{2} C_{DT} d \rho_w |\mathbf{v}\cdot\mathbf{t}|(\mathbf{v}\cdot\mathbf{t}) \\
\mathbf{f}_{dn} &= -\frac{1}{2} C_{DN} d \rho_w |\mathbf{v} - (\mathbf{v}\cdot\mathbf{t})\mathbf{t}|(\mathbf{v} - (\mathbf{v}\cdot\mathbf{t})\mathbf{t}) \\
\mathbf{f}_{a} &= -C_A \frac{\pi d^2}{4} \rho_w (\mathbf{a} - (\mathbf{a}\cdot\mathbf{t})\mathbf{t})
\end{aligned}$$

Where C_A, C_{DN} and C_{DT} are the added mass-, normal drag- and tangential drag coefficients of the mooring line, ρ_w and ρ_m are the density of water and mooring line and d is the cable diameter. $\mathbf{a} = \dot{\mathbf{v}}$ is the acceleration.

Since the partial differential equation (PDE) in (4.17) can not be solved directly, FEM may be used given by the following procedure:

[1] Calculate element lengths due to elongation based on top tension

[2] Correction of top node due to offset and current load

[3] Calculate external forces based on tension, weight and current load

[4] Get axial internal forces from position of each node, element length and elastic stiffness

For a mooring line of n segments of length $l = L/n$, like in Figure 4.6, the n coupled ordinary differential equations given by Aamo & Fossen (2001) are:

$$\frac{\rho_0 l}{6}\left(\ddot{\mathbf{r}}_{k-1} + 4\ddot{\mathbf{r}}_k + \ddot{\mathbf{r}}_{k+1}\right) + EA_0\left(\frac{e_k}{\epsilon_k}\mathbf{l}_k - \frac{e_{k+1}}{\epsilon_{k+1}}\mathbf{l}_{k+1}\right) = \mathbf{f}_{k,hg} + \mathbf{f}_{k,dt} + \mathbf{f}_{k,dn} \tag{4.18}$$

for $k = 1, 2, ..., n-1$. Drag domination has been assumed, and therefore added mass has been neglected. The following is used in (4.18)

$$\mathbf{f}_{k,hg} = l\rho_0\frac{\rho_c - \rho_w}{\rho_c}\begin{bmatrix}0 & 0 & g\end{bmatrix}^T$$

$$\mathbf{f}_{k,dt} = -\frac{C_1}{2}\left(|\dot{\mathbf{r}}_k \cdot \mathbf{l}_k|\mathbf{P}_k + |\dot{\mathbf{r}}_k \cdot \mathbf{l}_{k+1}|\mathbf{P}_{k+1}\right)\dot{\mathbf{r}}_k$$

$$\mathbf{f}_{k,dn} = -\frac{C_2}{2}\Big(\epsilon_k|\left(\mathbf{I}_{3\times3} - \mathbf{P}_k\right)\dot{\mathbf{r}}_k|\left(\mathbf{I}_{3\times3} - \mathbf{P}_k\right) + \epsilon_{k+1}|\left(\mathbf{I}_{3\times3} - \mathbf{P}_{k+1}\right)\dot{\mathbf{r}}_k|\left(\mathbf{I}_{3\times3} - \mathbf{P}_{k+1}\right)\Big)\dot{\mathbf{r}}_k$$

$$\mathbf{l_k} = \mathbf{r}_k - \mathbf{r}_{k-1}, \quad \epsilon_k = |\mathbf{l}_k|, \quad \mathbf{P}_k = \frac{\mathbf{l}_k\mathbf{l}_k T}{\epsilon_k^2}$$

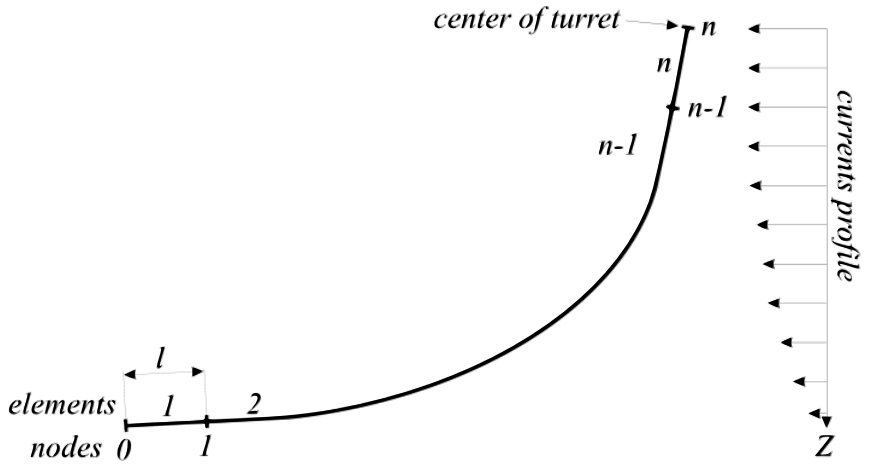

Figure 4.6: Elements on mooring line (hang-off at CoT)

Discretization

The number of elements the mooring line is divided into, depends on calculation time and how accurate a solution is desired. Typically, the segmentation at the seabed should be finer, due to friction effects, but the simulation time increases drastically when the number of elements is increased, especially when calculating for several mooring lines simultaneously.

In the interest of reducing the calculation time, for mooring systems with long segments of chain submerged into the seabed, the part of the mooring line considered in the analysis can be shortened. With this one is assuming that the chain will have no movement towards the anchor

after a certain length of submerged chain. This is a fair assumption for POSMOOR analysis, especially simulating moderate weather conditions.

In Figure 4.8 the resulting horizontal force of the cable simulated in Figure 4.7 is shown for 100 and 10 elements. The red line shows the results using coarse mesh but with a fine mesh of the bottom segment. For small horizontal displacement of the hang-off position, the latter solution follows the fine mesh solution very well. Since the horizontal displacement of the vessel is supposed to be small, this observation is relevant for a POSMOOR system.

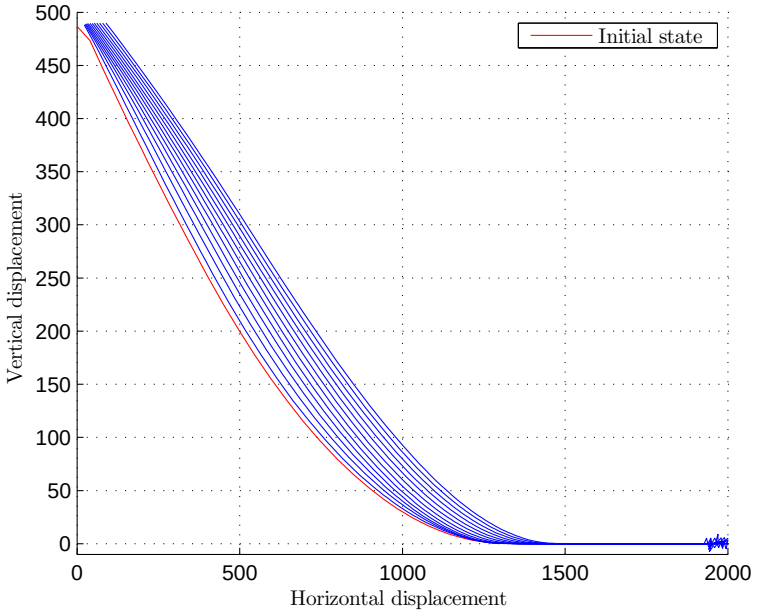

Figure 4.7: Simulation of mooring line in current

4.4.3 Modelling of the Mooring System

Like vessels, the modeling of a mooring system with m mooring lines, each divided into n segments, can be done by combining equation (4.4) and (4.6). Defining a relative velocity $\mathbf{v}_j^i = \dot{\mathbf{r}}_j^i - \mathbf{v}_c$ between the velocity of the kth node of the jth mooring line and the fluid velocity $\mathbf{v}_c$, the ODE[1] for each node, k, on each mooring line, j, can be written as

$$\mathbf{M}_k^j \dot{\mathbf{v}}_k^j + \mathbf{D}_k^j \mathbf{v}_k^j + \mathbf{k}_k^j + \mathbf{g}_k^j = \mathbf{0} \tag{4.19}$$

When this is coupled with the vessel dynamics (4.8), the inertia, drag and hydrostatic and gravitation effects in (4.19) are so small relative to the ones for the vessel, so that they can be neglected. The restoring force is given by

$$\mathbf{k}_k^j = \frac{E_j A_{0,j}}{l_j} \left(\frac{\epsilon_k^j - l_j}{\epsilon_k^j} \mathbf{l}_k^j - \frac{\epsilon_{k+1}^j - l_j}{\epsilon_{k+1}^j} \mathbf{l}_{k+1}^j \right)$$

[1] Ordinary differential equation

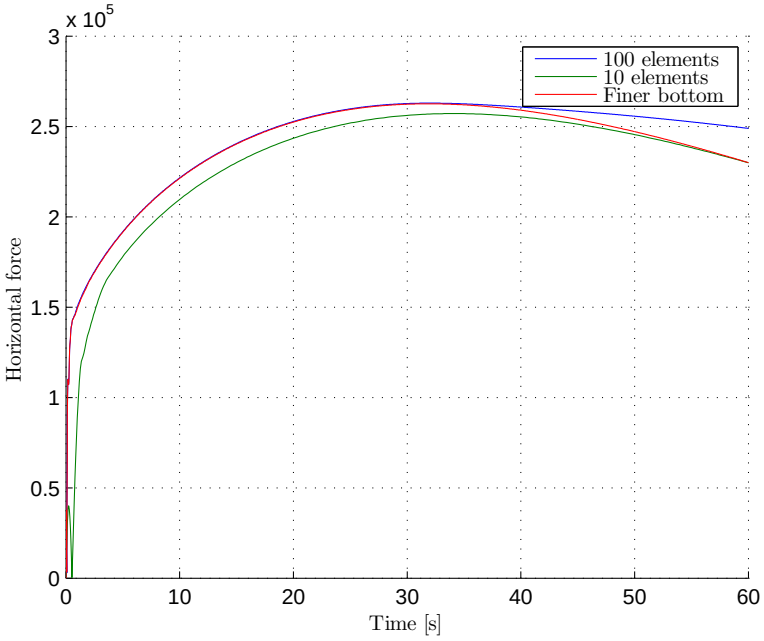

Figure 4.8: Horizontal force and number of elements

The kinematics (4.1) gives

$$\mathbf{r}_n^j = \boldsymbol{\eta}_1 + \mathbf{J}_1(\boldsymbol{\eta}_2)\mathbf{p}^j$$
$$\mathbf{v}_n^j = \mathbf{J}_1(\boldsymbol{\eta}_2)\boldsymbol{\nu}_1 + \frac{d}{dt}\left(\mathbf{J}_1(\boldsymbol{\eta}_2)\mathbf{p}^j\right)$$

where $\boldsymbol{\eta}_1 = [x\ y\ z]^T$, $\boldsymbol{\eta}_2 = [p\ q\ r]^T$, $\boldsymbol{\nu}_1 = [u\ v\ w]^T$, $\boldsymbol{\eta}_1 = \mathbf{J}_1(\boldsymbol{\eta}_2)\boldsymbol{\nu}_1$ and $\mathbf{p}^j$ is the point on the ship at which mooring line j is connected. Resulting in the mooring force

$$\boldsymbol{\tau}_{mooring} = \begin{bmatrix} \sum_{j=1}^{m} \mathbf{J}_1(\boldsymbol{\eta}_2)\mathbf{k}_n^j \\ \sum_{j=1}^{m} \left(\mathbf{J}_1(\boldsymbol{\eta}_2)\mathbf{k}_n^j\right) \times \mathbf{p}^j \end{bmatrix} \tag{4.20}$$

4.5 Risers

Since the purpose of the mooring system is to reduce the motions of the vessel, and therefore the loads on the risers, the risers influence in the horizontal plane should be small compared to that of the mooring and the vessel. The risers influence can therefore be represented by a vertical load acting on the turret for the applications considered. This simplification becomes less applicable when you have large numbers of risers and umbilicals.

Chapter 5

Control

Motion control is the action of determining the necessary control forces and moments to be provided by the craft in order to satisfy a certain control objective (Fossen 2011).

PID-based control can be used to control the horizontal motions of the vessel with three decoupled PID controllers, giving commands to thrusters and propellers.

5.1 Control Objective

In order to design an efficient motion control system, the control objective must be clear and well defined, since it sets the requirements the system. For a POSMOOR system, the requirements for stationkeeping are not as strict as for a DP system, as the purpose is mainly to assist the mooring system. For moderate weather conditions, the control objective can be divided into two parts

1. Provide damping in surge and sway when large motions occur
2. Keep the vessel at an optimal heading for weather waning

Additionally, if the weather conditions should become so harsh that the risk of mooring line breakages , damping in surge and sway is no longer be sufficient. In this case, the objective of the POSMOOR system is extended to keeping the vessel within a safe range in terms of mooring line tension.

5.2 Control Plant Model

Examining the control objective of the POSMOOR system, it is apparent that the control is only needed in the horizontal plane. The system (4.8) can therefore be reduced to 3 DOF[1], namely surge, sway and yaw. Furthermore, the vessel velocities for stationkeeping are small, which allows for neglecting the Coriolis and sentripetal terms along with the nonlinear damping.

[1] Degrees of Freedom

5.2.1 Control Plant Model - LF

The assumtions made allows the low-frequency model from (4.8) to be reduced to

$$\begin{aligned}\dot{\boldsymbol{\eta}} &= \mathbf{R}(\psi)\boldsymbol{\nu} \\ \dot{\mathbf{b}} &= -\mathbf{T}_b^{-1}\mathbf{b} + \mathbf{E}_b\mathbf{w}_b \\ \mathbf{M}\dot{\boldsymbol{\nu}} &= -\mathbf{D}\boldsymbol{\nu} + \mathbf{R}^T(\psi)\mathbf{b} + \boldsymbol{\tau}_{mooring} + \boldsymbol{\tau}_{thrust}\end{aligned} \tag{5.1}$$

Where the rotation matrix

$$\mathbf{R}(\psi) = \begin{bmatrix} c\psi & -s\psi & 0 \\ s\psi & c\psi & 0 \\ 0 & 0 & 1 \end{bmatrix} \tag{5.2}$$

has the property $\mathbf{R}^{-1}(\psi) = \mathbf{R}^T(\psi)$. The bias term, $\mathbf{b}$, includes slowly varying disturbances and dynamics that are not accounted for. $\boldsymbol{\tau}_{thrust}$ is the control force vector given in the body-fixed reference frame.

The mooring system load on the vessel can be modelled by a restoring force and a damping force (Sørensen (2011)), and is given by

$$\boldsymbol{\tau}_{mooring} = -\mathbf{J}^{-1}(\boldsymbol{\eta})\mathbf{G}_{mooring}(\boldsymbol{\eta}) - \mathbf{D}_{mooring}(\boldsymbol{\nu}_r) \tag{5.3}$$

The mooring force from (5.3) is reduced to 3DOF, so that

$$\boldsymbol{\tau}_{mooring} = -\mathbf{R}^T(\psi)\mathbf{G}_{mooring}(\boldsymbol{\eta}) - \mathbf{D}_{mooring}(\boldsymbol{\nu}_r) \tag{5.4}$$

Since small velocities were assumed, (5.4) can be approximated by a first order Tailor expansion about a working point $\boldsymbol{\nu}_r = \boldsymbol{\nu} = \mathbf{0}$, $\boldsymbol{\eta}_0 = \boldsymbol{\eta}$, so that

$$\begin{aligned}\boldsymbol{\tau}_{mooring} =& -\mathbf{R}^T(\psi)\frac{\delta \mathbf{G}_{mooring}(\boldsymbol{\eta})}{\delta \boldsymbol{\eta}}\bigg|_{\boldsymbol{\eta}=\boldsymbol{\eta}_0}(\boldsymbol{\eta}-\boldsymbol{\eta}_0) \\ & - \frac{\delta \mathbf{D}_{mooring}(\boldsymbol{\nu})}{\delta \boldsymbol{\eta}}\bigg|_{\boldsymbol{\nu}=\mathbf{0}}\boldsymbol{\nu} \\ =& -\mathbf{R}^T(\psi)\mathbf{G}'_{mooring}\boldsymbol{\eta} - \mathbf{D}'_{mooring}\boldsymbol{\tau}_c\boldsymbol{\nu} \qquad (5.5) \\ & \qquad (5.6)\end{aligned}$$

The resulting LF model is

$$\begin{aligned}\dot{\boldsymbol{\eta}} &= \mathbf{R}(\psi)\boldsymbol{\nu} \\ \dot{\mathbf{b}} &= -\mathbf{T}_b^{-1}\mathbf{b} + \mathbf{E}_b\mathbf{w}_b \\ \mathbf{M}\dot{\boldsymbol{\nu}} &= -\mathbf{D}\boldsymbol{\nu} + \mathbf{R}^T(\psi)\mathbf{b} - \mathbf{R}^T(\psi)\mathbf{G}'_{mooring}\boldsymbol{\eta} + \boldsymbol{\tau}_c\end{aligned} \tag{5.7}$$

Where the damping term from the mooring load (5.5) has been added to $\mathbf{D}$.

5.2.2 Control Plant Model - WF

The wave frequency part of the control plant model is obtained by assuming that (4.9) takes the form (Sørensen 2013)

$$\dot{\boldsymbol{\xi}}_w = \mathbf{A}_w\boldsymbol{\xi}_w + \mathbf{E}_w\mathbf{w}_w \tag{5.8}$$

$$\boldsymbol{\eta}_w = \mathbf{C}_w\boldsymbol{\xi}_w \tag{5.9}$$

where

$$\mathbf{A}_w = \begin{bmatrix} \mathbf{0}_{3\times3} & \mathbf{I}_{3\times3} \\ -\mathbf{\Omega}^2 & -2\mathbf{\Lambda}\mathbf{\Omega} \end{bmatrix}, \qquad \mathbf{C}_w = \begin{bmatrix} \mathbf{0}_{3\times3} & \mathbf{I}_{3\times3} \end{bmatrix}, \qquad \mathbf{E}_w = \begin{bmatrix} \mathbf{0}_{3\times3} \\ \mathbf{K}_w \end{bmatrix}$$

The system matrix, $\mathbf{A}_w$, corresponds to a mass-damper-spring description of the wave frequency induced motion (Response Amplitude Operators). $\mathbf{\Omega}$ is a diagonal matrix containing the dominating wave response frequencies in the given sea state and $\mathbf{\Lambda}$ contains damping ratios.

5.3 Nonlinear Passive Observer Design

The forces induced at wave difference frequencies can have low frequency content, which may cause resonance in the horizontal motion of position moored vessels (Faltinsen 1990). Controlling for correcting the motion induced by every single wave, however, can result in unacceptable operational conditions for the propulsion system both in terms of wear and power consumption.

A cascaded notch and a low-pass filter, also known as a *wave filter*, can be used to remove the oscillatory part of the measurements by preventing the first order wave induced motions from entering the feedback loop with the heading and position measurement. By feeding the filtered signal to the controller, only the lower frequency motions are accounted for by the POSMOOR system.

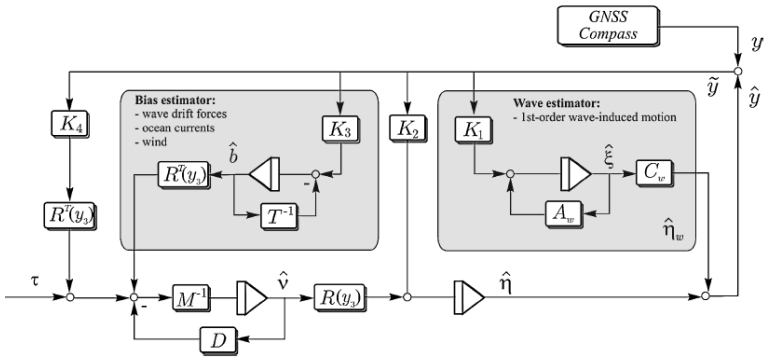

Figure 5.1: Nonlinear Passive Observer block diagram (Sørensen 2013)

The *nonlinear passive observer* described in Sørensen (2013), can be used for wave filtering in addition to velocity and bias estimation. The nonlinear observer has far less parameters to tune, compared to the *Extended Kalman filter*.

The observer equations corresponding with Figure 5.1 are:

$$\dot{\hat{\boldsymbol{\xi}}} = \mathbf{A}_w\hat{\boldsymbol{\xi}} + \mathbf{K}_1\tilde{\mathbf{y}}, \tag{5.10}$$

$$\dot{\hat{\boldsymbol{\eta}}} = \mathbf{R}(\psi_y)\hat{\boldsymbol{\nu}} + \mathbf{K}_2\tilde{\mathbf{y}}, \tag{5.11}$$

$$\dot{\hat{\mathbf{b}}} = -\mathbf{T}_b^{-1}\hat{\mathbf{b}} + \mathbf{K}_3\tilde{\mathbf{y}}, \tag{5.12}$$

$$\mathbf{M}\dot{\hat{\boldsymbol{\nu}}} = -\mathbf{D}\hat{\boldsymbol{\nu}} - \mathbf{R}^T(\psi_y)\mathbf{G}'_{mooring}\hat{\boldsymbol{\eta}} + \mathbf{R}^T(\psi_y)\hat{\mathbf{b}} + \boldsymbol{\tau}_c + \mathbf{R}^T(\psi_y)\mathbf{K}_4\tilde{\mathbf{y}} \tag{5.13}$$

5.4 Thrust Allocation

The generalized control forces, $\boldsymbol{\tau}_{thrust}$, needs to be distributed to the actuators in terms of control inputs, $\mathbf{u}$. CS3 has a propulsion cofiguration consisting of three azimuth thrusters, two in the back and one in front, and one tunnel thruster in front (see Figure 5.2)

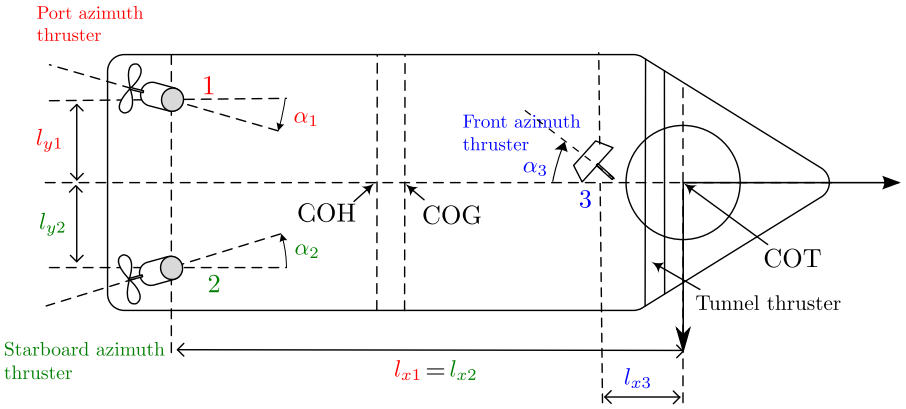

Figure 5.2: Thruster configuration for CS3

Using the method described by Fossen (2011), the control forces and moment can be expressed by the control vector, $\mathbf{f} = \begin{bmatrix} F_x, F_y, F_z \end{bmatrix}^T$ and the corresponding moment arms $\mathbf{r} = \begin{bmatrix} l_x, l_y, l_z \end{bmatrix}^T$

$$\boldsymbol{\tau}_{thrust} = \begin{bmatrix} \mathbf{f} \\ \mathbf{r} \times \mathbf{f} \end{bmatrix} = \begin{bmatrix} F_x \\ F_y \\ F_z \\ F_z l_y - F_y l_z \\ F_x l_z - F_z l_x \\ F_y l_x - F_x l_y \end{bmatrix} \overset{3DOF}{=} \begin{bmatrix} F_x \\ F_y \\ F_y l_x - F_x l_y \end{bmatrix} \tag{5.14}$$

the relationship between $\mathbf{f}$ and the control input is written

$$\mathbf{f} = \mathbf{K}\mathbf{u} \tag{5.15}$$

where $\mathbf{K} = diag\{K_1, ..., K_r\}$ is a diagonal force coefficient matrix relating to the r actuators. For a marine craft with p rotatable thrusters with azimuth angles, $\boldsymbol{\alpha} = \begin{bmatrix} \alpha_1, ..., \alpha_p \end{bmatrix}^T$, we introduce the thrust configuration matrix $\mathbf{T}(\boldsymbol{\alpha})$, so that

$$\boldsymbol{\tau}_{thrust} = \mathbf{T}(\boldsymbol{\alpha})\mathbf{K}\mathbf{u} \tag{5.16}$$

where

$$\mathbf{T}(\boldsymbol{\alpha}) = \begin{bmatrix} \mathbf{t}_1, ..., \mathbf{t}_r \end{bmatrix} = \begin{bmatrix} \cos(\alpha_1) & & \\ \sin(\alpha_1) & & , ..., \mathbf{t}_r \\ l_{x1}\sin(\alpha_1) - l_{y1}\cos(\alpha_1) & & \end{bmatrix} \tag{5.17}$$

For a tunnel thruster

$$\mathbf{t}_i = \begin{bmatrix} 0 \\ 1 \\ l_{xi} \end{bmatrix} \tag{5.18}$$

Quantity	Symbol	Unit	Value
Port azimuth thruster (1)			
Thrust characteristics in positive rpm	$k_{T0,p1}$	N/rpm^2	$6.544 \cdot 10^{-6}$
Thrust characteristics in negative rpm	$k_{T0,n1}$	N/rpm^2	$4.521 \cdot 10^{-6}$
Maximum rpm	$n_{max,1}$	rpm	$1.2 \cdot 10^3$
Location with respect to COT	(l_{x1}, l_{y1})	m	$(-1.72, -0.11)$
Starboard azimuth thruster (2)			
Thrust characteristics in positive rpm	$k_{T0,p2}$	N/rpm^2	$6.464 \cdot 10^{-6}$
Thrust characteristics in negative rpm	$k_{T0,n2}$	N/rpm^2	$4.482 \cdot 10^{-6}$
Maximum rpm	$n_{max,2}$	rpm	$1.2 \cdot 10^3$
Location with respect to COT	(l_{x2}, l_{y2})	m	$(-1.72, 0.11)$
Front azimuth thruster (3)			
Thrust characteristics in positive rpm	$k_{T0,p3}$	N/rpm^2	$1.512 \cdot 10^{-6}$
Thrust characteristics in negative rpm	$k_{T0,n3}$	N/rpm^2	$6.046 \cdot 10^{-7}$
Maximum rpm	$n_{max,3}$	rpm	$2.0 \cdot 10^3$
Location with respect to COT	(l_{x3}, l_{y3})	m	$(-0.19, 0.0)$

Table 5.1: Parameters for CS3's thrusters

The thrust allocation has been implemented in simulink, but serve no actual purpose since the inverse relationship is used within the process plant model. To reduce calculation time, the calculated

5.4.1 Reference Generation

One control objective is to provide damping to the motions in surge and sway. In other words, the mooring system should provide the main contribution to restraining the vessel offset. By using reference models motivated by the dynamics of mass-spring-damper systems, one can generate suitable trajectories for marine vessels, by assuming the desired setpoint (SP) to be the lowpass signal of the LF position vector. When wind measurements are available, it is common to use the wind direction, for the desired heading. Since the wind direction is constant in this assignment, the filtering will be used for the surge and sway positions only.

Setpoint Chasing

Nguyen & Sorensen (2009) proposed a strategy for setpoint (SP) generation for POSMOOR systems in moderate to extreme seas, which has been tested in the model. Looking back at the control objectives, as the offset of the vessel becomes so large that the safety region of the mooring line tension is transcended, action must be taken to avoid loss of mooring lines. By defining a SP for extreme conditions $\boldsymbol{\eta}_{cr}$ one can avoid that the tension in any of the mooring lines reaches its critical region.

The mooring line tension in line i with associated lay-down angle, is determined by the horizontal distance according to (Nguyen & Sorensen 2009)

$$T_i = f(X_i^{hor}) \tag{5.19}$$

But can also be directly measured. Monitoring of the line-tensions is normal on turret-mooring configurations.

Reference model

In order to avoid sudden changes in the reference position as the setpoint changes, third order low-pass filters for smooth transition has been applied. The filters are first order low-pass filters in cascade with a spring-mass-damper model like described in for example (Sørensen 2013). The filters are defined by the transfer function:

$$\frac{\eta_{di}}{r_i^n}(s) = \frac{\omega_{ni}^2}{(1+T_{is})(s^2+2\zeta_i\omega_{ni}s+\omega_{ni}^2)} \tag{5.20}$$

Velocity saturation has also been used for additional improvement (Sørensen 2013).

5.4.2 Controller

PID (proportional, derivative and integral) control has been applied for the horizontal degrees of freedom. The controller gains have been tuned through simulations to best satisfy the control objectives. The controller gain in COT based on the LF positions in NED, is given by

$$\boldsymbol{\tau}_c = \mathbf{K}_p\mathbf{R}^T(\psi_y)(\boldsymbol{\eta}_d - \boldsymbol{\eta}) - \mathbf{K}_d\mathbf{R}^T(\psi_y)\boldsymbol{\nu} - \mathbf{K}_i\int \mathbf{R}^T(\psi_y)(\boldsymbol{\eta}_d - \boldsymbol{\eta}) \tag{5.21}$$

where $\boldsymbol{\eta}_d = [N_d E_d \psi_d]^T$ is the desired position and heading of the vessel. The gain matrices have been chosen to be diagonal in this assignment, as the off-diagonal values provide 36 parameters to tune all together, which is extreme when tuning by simulating. There are however software for PID tuning that could make it possible, further impoving the handling between the NE position and the yaw angle.

Chapter 6

Simulations and Results

A 6 DOF model of a mooring system applied to CS3, like described in chapter 4, was implemented in simulink during the preliminary assignment, as was used as a basis for the model made in this thesis. The diagrams and code can be found in **??**, and a more complete set of plots in Appendix C.

6.1 Improvement of the Old Model

From the previous assignment, the convergence of the FEM on the mooring lines was poor, and the tension measurements were unusable. The problem turned out to be the horizontal seabed interaction, which for simulations of a single mooring line was fine, as can be seen in Figure 6.1. The horizontal seabed friction effect was therefore removed from the model. Since the current

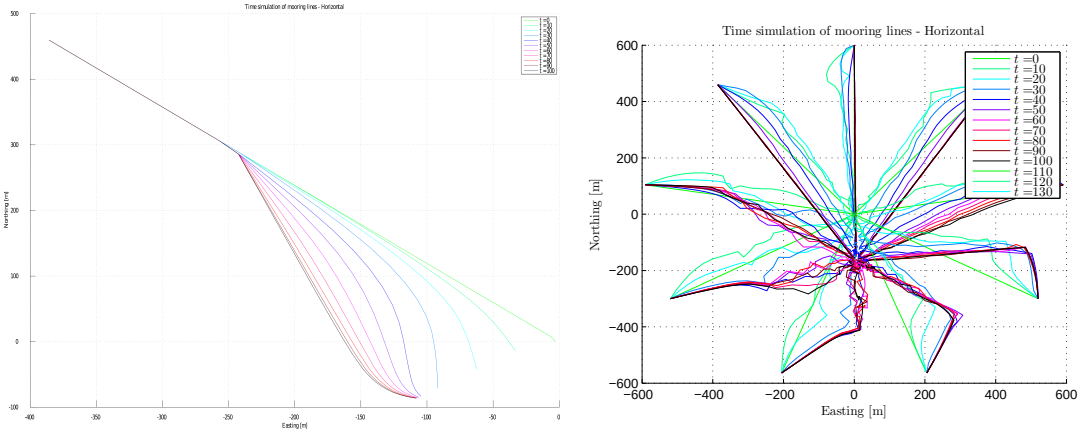

Figure 6.1: Seabed friction included

has now been given a varying profile, this should not make too much of a difference.

6.2 Determining the Influence from the Mooring System

Decay tests were run while neglecting the damping and restoring forces of the vessel, in order to determine the damping and restoring in Equation 5.5 for north and east, to use in the Observer. Since the vessel is turret moored, it is assumed to be able to rotate freely around the turret, and the contributions in yaw has therefore been put to zero. The equation of an underdamped system is given by

$$x(t) = e^{-\zeta\omega_0 t}(A\cos(\omega_d t) + B\sin(\omega_d t)) \tag{6.1}$$

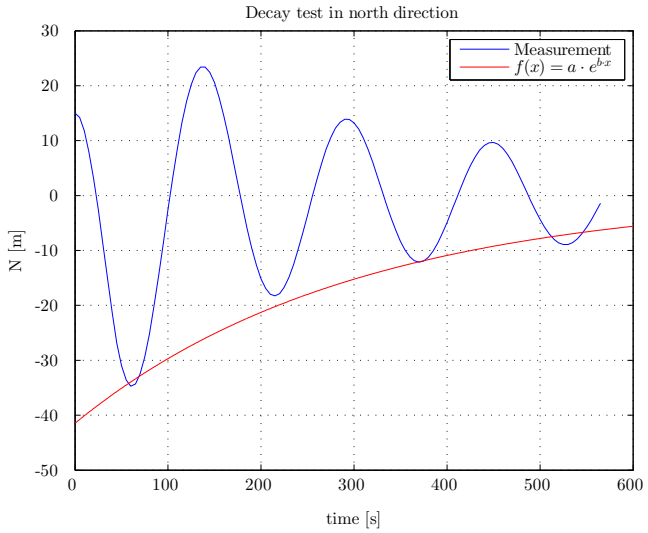

Figure 6.2: Result of decay test in north direction

By examining the free oscillation, the damping coefficient, ζ, can be found by curvefitting the displacement peaks (or troughs) with an exponential function. The period $T_d = \frac{2\pi}{\omega_d}$ is the time between the peaks or troughs, and the undamped angular frequency, ω_0 is given by

$$\omega_d = \omega_0\sqrt{1-\zeta^2} \qquad\qquad \omega_0 = \sqrt{\frac{k}{m}} \tag{6.2}$$

A constant force was applied in the direction in question at $t = [0, 60]$, and the oscillations back to equilibrium was observed like in Figure 6.2. Since the mooring system consists of nine lines and is therefore only symmetrical about the ND plane, the $G_{mooring}$ and $D_{mooring}$ will have contributions in the north direction for movement in east. Geometry yields:

$$\tau_{mooring}(2,2) = \sin\left(\frac{4\pi}{9}\right)\cdot\tau_{mooring}(1,1)$$
$$\tau_{mooring}(2,1) = \cos\left(\frac{4\pi}{9}\right)\cdot\tau_{mooring}(1,1)$$

$$\mathbf{G}^{3DOF}_{mooring} = \begin{bmatrix} 3\,388 & 0 & 0 \\ 588.2 & 3\,336.5 & 0 \\ 0 & 0 & 0 \end{bmatrix} \qquad \mathbf{D}^{3DOF}_{mooring} = \begin{bmatrix} 13\,857 & 0 & 0 \\ 2\,406 & 13\,646 & 0 \\ 0 & 0 & 0 \end{bmatrix}$$

Parameter	Unit	(1,1)	(2,2)	(2,1)
T_d	[s]	155	155	155
$G_{mooring}$	[N/m]	3 388	3 336.5	588.2
$D_{mooring}$	[Ns/m]	13 857	13 646	2 406

Table 6.1: Results from decay test

6.3 Uncontrolled System with Environmental Loads

In order to investigate how the mooring lines now behave under the influence of current, a simulation case was run with unrealistically large current, vessel fixed in the equilibrium position.

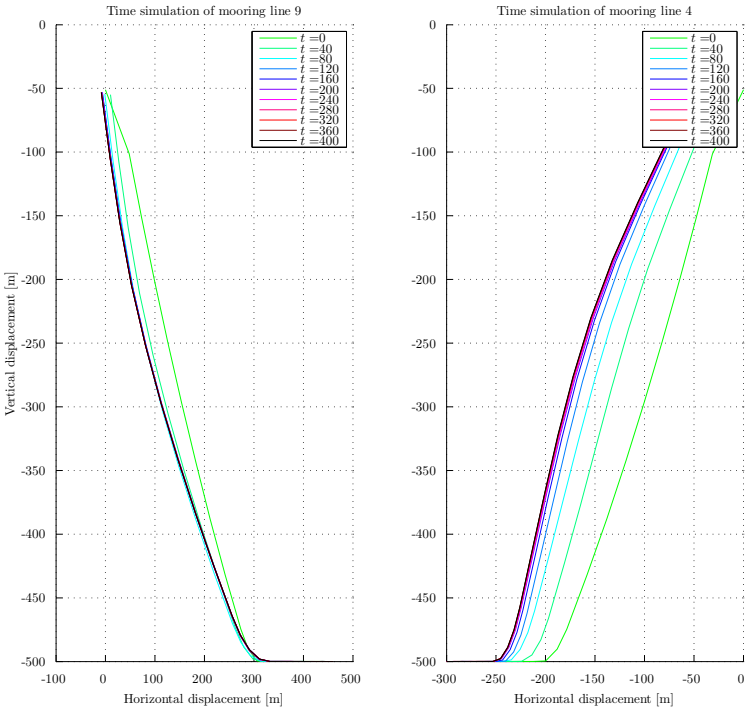

Figure 6.3: Mooring line drag

As can be seen in Figure 6.3, the stability of the FEM solver is now excellent, even for very large currents.

The weather waning capability, now with the equations of motions calculated in COT, was also verified to see that the conversion was done correctly. Notably, the friction effect from the turret itself is not included in the model, so that the weather waning capability is much more limited in reality.

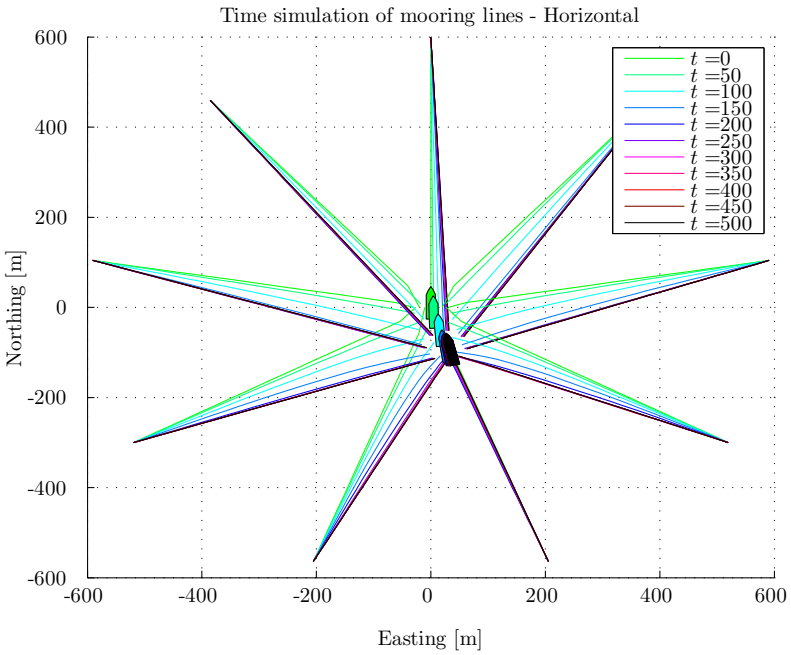

Figure 6.4: Weather waning in bidirectional current and wind)

$\mathbf{V_c}$ $[m/s]$	$\boldsymbol{\beta_c}$ $[deg]$	$\mathbf{V_w}$ $[m/s]$	$\boldsymbol{\beta_w}$ $[deg]$
0.2	165	14	175

Table 6.2: Environmental data

6.4 Observer performance

The model was modified to including the wave frequency motions based on motion RAOs found in , in order to tune a nonlinear passive observer. Current and wind forces are not included, to investigate the effects of the wave drift forces.

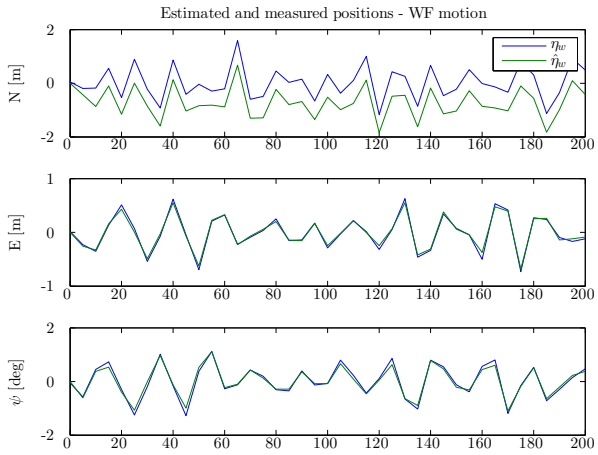

Figure 6.5: Wave estimate

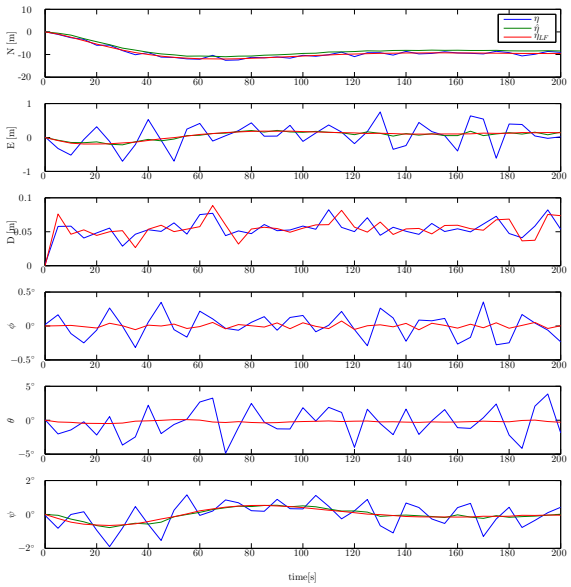

Figure 6.6: Position and orientation with wave filtering

The estimates are good, however a small part of the lower frequency motion is being filtered out along with the wave estimates, most notably in the north direction in Figure 6.5, which is the dominant direction of the waves. Compared with the total wave drift force that can be seen in Figure 6.6, this is tolerable.

6.5 Reference Model and Control

The POSMOOR system was subjected to the same environmental loads as in Figure 6.4. The trajectories of the reference model are very smooth and the controller follow them well as can be seen in Figure 6.7. The transition is well handled by the reference system and the controller.

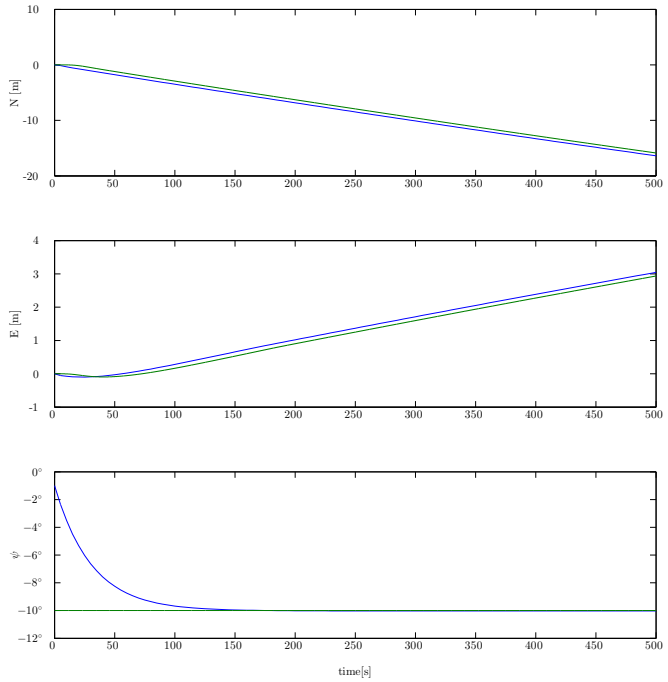

Figure 6.7: Positions and references

6.5.1 Extreme Weather SP transition

A position, $\boldsymbol{\eta}_c = 50\ [m]$ was investigated in terms of transition between set points. The switching can be observed at $t = 360s$

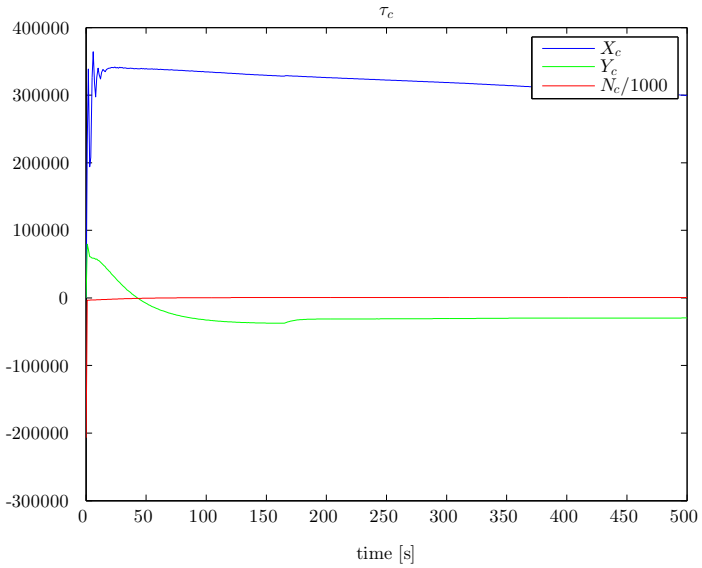

Figure 6.8: Thrust Output

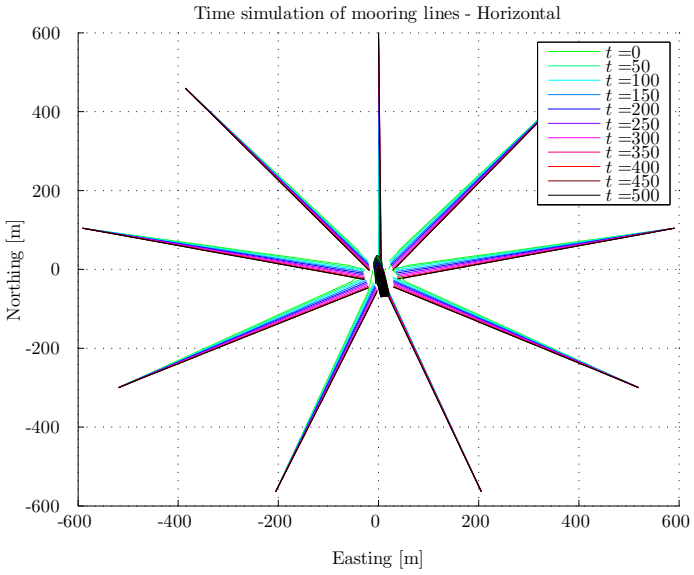

Figure 6.9: The moored vessel during transition to new set-point

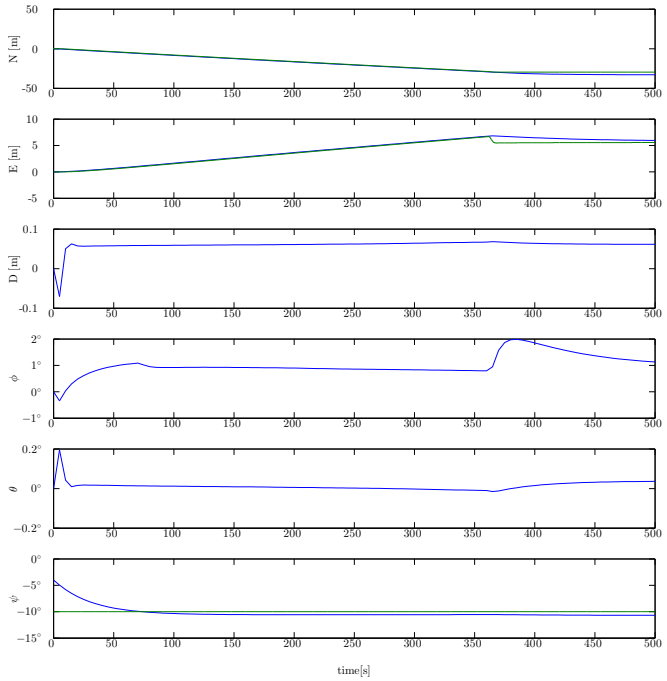

Figure 6.10: Trajectory, reference and LF measurement

Chapter 7

Concluding Remarks

7.1 Conclusion

During the work on this project, the basis of the POSMOOR system for CS3 started on during the fall of 2013 has been expanded and improved based on studies of available litterature. Different mooring- and turret configurations and when to apply them has been discussed.

A mooring system has been suggested, for which specifications have been worked out and listed. From these specifications, vessel- and mooring system kinematics and dynamics have been formulated and implemented in Matlab/Simulink. Simulations have been run on the Simulink model to tune an Observer, a reference model and PID control.

The model seems to work properly, and simulates quickly. For the purpose of POSMOOR simulations, the accuracy of the solution is satisfactory.

The reference model may be a bit strict, as the thrust output is quite large and offsets relatively small compared to depth and enviornmental loads.

Fo The finite element method seems suitable for the mooring lines, and the shape of the lines seems very reasonable although the friction on the seabed had to be neglected.

7.2 Further Work

The POSMOOR system is far from being applicable. Multiple controllers and setpoint generation for other operations modes than here presented should be implemented. Fault tolerant control is also very applicable on the model, now that the measurements has been improved

The FEM model on the mooring lines could be altered to include the MLBEs with characteristics such as drag, to get a better picture on how the mooring lines would behave, or for appliance of a fault tolerant control system structure with loss of MLBE as a failure mode. The thrust allocation can also be added within the model with thruster characteristics. This will provide more accurate behaviour in terms of the thrust output, and also apply the limitation in terms of thrust output.

Bibliography

Aamo, O. M. & Fossen, T. I. (2001), 'Finite element modelling of moored vessels', *Mathematical and Computer Modelling of Dynamical Systems* **7**(1), 47–75.

Aanesland, V., Kaalstad, J., Bech, A. & Holm, A. (2007), Disconnectable fpso-technology to reduce risk in gom, *in* 'Offshore Technology Conference'.

Barth Berntsen, P., Aamo, O. M. & Leira, B. J. (2008), 'Thruster assisted position mooring based on structural reliability', *International Journal of Control* **81**(9), 1408–1416.

Berntsen, P. I. B. (2008), Structural reliability based position mooring, PhD thesis, Norwegian University of Science and Technology, Department of Marine Technology, Trondheim, Norway.

Boatman, L. T., McCollum, J. L. & Garnero, C. L. (2006), 'Large diameter mooring turret with compliant deck and frame'. US Patent 6,990,917.

Dong, N. T. (2006), Design of hybrid marine control systems for dynamic positioning, PhD thesis.

Faltinsen, O. M. (1990), *Sea Loads on Ships and Offshore Structures*, Cambridge University Press.

Fossen, T. I. (2011), *Handbook of Marine Craft Hydrodynamics and Motion Control*, John Wiley & Sons.

Howell, G. B., Duggal, A. S., Heyl, C. & Ihonde, O. (2006), Spread moored or turret moored fpso's for deepwater field developments.

Nguyen, D. T. & Sorensen, A. J. (2009), 'Setpoint chasing for thruster-assisted position mooring', *Oceanic Engineering, IEEE Journal of* **34**(4), 548–558.

Rustad, A. M. (2013), 'Modeling and control of top tensioned risers'. Lecture notes in TMR4515 Module A, Department of Marine Technology, Norwegian University of Science and Technology, Trondheim, Norway.

Sørensen, A. J. (2011), 'A survey of dynamic positioning control systems', *Annual reviews in control* **35**(1), 123–136.

Sørensen, A. J., Strand, J. P. & Fossen, T. I. (1999), Thruster assisted position mooring system for turret-anchored fpso's, *in* 'Control Applications, 1999. Proceedings of the 1999 IEEE International Conference on', Vol. 2, IEEE, pp. 1110–1117.

Sørensen, A. J. (2013), *Marine Control Systems - Propulsion and Motion Control on Ships and Offshore Structures*, Department of Marine Technology, Norwegian University of Science and Technology, Trondheim, Norway.

Steen, S. (2013), 'Scaling laws'. Lecture notes in TMR 7 Experimental methods in Marine Hydrodynamics , Department of Marine Technology, Norwegian University of Science and Technology, Trondheim, Norway.

Strand, J. P., Sørensen, A. J. & Fossen, T. I. (1998), 'Design of automatic thruster assisted position mooring systems for ships', *Modeling, identification and control* **19**(2), 61–75.

Wichers, J. (2013), *Guide to Single Point Moorings*, WMooring.

Appendix A

Norwegian Summary

Denne avhandlingen er et studie på forankringssystemer på flytende produksjon, lagring, lossing (FPSO) enheter, og omfatter en undersøkelse av POSMOOR system. En modell som inneholder et thruster assistert posisjon fortøyning (POSMOOR) system har blitt utredet og implementert i matlab/Simulink. En diskusjon av hva slags forankringssystem som er mest passende for ulike forhold presenteres i innledningen, etterfulgt av et eksempel på en turret fortøyd enhet. Bevegelseslikninger i seks frihetsgrader har blitt beskrevet og implementert i Matlab / Simulink, ved hjelp av parametere gitt av Marine Cybernetics Lab, på Cybership III. Noen av disse parametrene er grove estimater eller svært usikre, og kan bli oppdatert i løpet av senere arbeid. Ankerlinenes dynamikk er beskrevet ved hjelp av elementmetoden, basert på arbeid utført av Ole Morten Aamo på ABB Integrert Vessel Simulator, og integrert i Simulink modell. Ni ankerliner blir simulert sammen med resten av modellen for å gi et godt bilde på hvordan systemet oppfører seg. Simuleringer ble gjort for å vise at forankringslinenes dynamikk er beskrevet på riktig måte, og for å se hvor godt skipet retter seg inn etter dominerende miljøbelastninger (Weatherwaning). Dette bekreftet at modellen fungerer etter hensikten og at FEM på linene er meget stabil Kontroll målet er blitt fastsatt, og basert på dette har POSMOOR systemet tatt form. Bølgefilter og biasestimasjon er implementert og tunet for å estimere de lavfrekvente bevegelsene ut fra målingene. En enkel setpoint modell basert på mooring linenes belastning er etablert for å unngå overbelastning av linene under ekstreme værforhold. For å generere en jevn overgang mellom ulike setpoints, har en referanse model blitt implementert og tunet. Kontroll med proporsjonal-,integral- og derivant (PID) virkning har blitt tunet.

Appendix B

Vessel Data

B.1 Main Parameters

Parameter	Unit	Model	Full Scale
Scale	[-]	1 : 30	-
Length between perpendiculars	[m]	1.971	59.13
Breadth	[m]	0.437	13.11
Draft	[m]	0.153	4.59
Displacement	[m^3]	0.075	2 025
Transverse metacentric height	[m]	0.02	0.60
Longship metacentric height	[m]	1.474	44.22
Waterplane area	[m^2]	0.656	590.4
Radius of gyration, roll	[m]	0.1713	5.139
Radius of gyration, pitch	[m]	0.5138	15.414
Radius of gyration, yaw	[m]	0.5138	15.414
Projected wind force area, surge (rough estimate)	[m^2]	0.0677	60.93
Projected wind force area, sway (rough estimate)	[m^2]	0.4	360
Projected current force area, surge	[m^2]	0.0620	55.8
Projected current force area, sway	[m^2]	0.25	225

Table B.1: CS3 main perpendiculars, model- and full scale

Rigid body mass:

$$\mathbf{M}_{RB} = \begin{bmatrix} 76.875 & 0 & 0 & 0 & -3.3056 & 0 \\ 0 & 76.875 & 0 & 3.3056 & 0 & 2.7675 \\ 0 & 0 & 76.875 & 0 & -2.7675 & 0 \\ 0 & 3.3056 & 0 & 2.3979 & 0 & 0.119 \\ -3.3056 & 0 & -2.7675 & 0 & 20.536 & 0 \\ 0 & 2.7675 & 0 & 0.119 & 0 & 20.394 \end{bmatrix} \tag{B.1}$$

Added mass:

$$\mathbf{M}_A = \begin{bmatrix} 0.006 & 0 & 0 & 0 & 0 & 0 \\ 0 & 72.7 & 0 & -2.74 & 0 & -3.84 \\ 0 & 0 & 160 & 0 & -5.9 & 0 \\ 0 & -2.74 & 0 & 0.433 & 0 & -0.322 \\ 0 & 0 & -5.9 & 0 & 27.9 & 0 \\ 0 & -3.84 & 0 & -0.322 & 0 & 13.7 \end{bmatrix} \tag{B.2}$$

Restoring forces and moments:

$$\mathbf{G} = \begin{bmatrix} 0 & 0 & 0 & 0 & 0 & 0 \\ 0 & 0 & 0 & 0 & 0 & 0 \\ 0 & 0 & 6596.2 & 0 & -237.46 & 0 \\ 0 & 0 & 0 & 15.083 & 0 & 0 \\ 0 & 0 & -237.46 & 0 & 1120.2 & 0 \\ 0 & 0 & 0 & 0 & 0 & 0 \end{bmatrix} \tag{B.3}$$

Linear damping:

$$\mathbf{D}_L = \begin{bmatrix} 12.203 & 0 & 0 & 0 & 0 & 0 \\ 0 & 11.871 & 0 & -0.0954 & 0 & 0.5852 \\ 0 & 0 & 453 & 0 & -28.808 & 0 \\ 0 & -0.0954 & 0 & 0.0059888 & 0 & -0.063004 \\ 0 & 0 & -28.808 & 0 & 81.087 & 0 \\ 0 & 0.5852 & 0 & -0.063004 & 0 & 4.371 \end{bmatrix} \tag{B.4}$$

B.2 Wind Coefficients

$\gamma_{\mathbf{rw}}$ [deg]	$\mathbf{C_X}(\gamma_{\mathbf{rw}})$	$\mathbf{C_Y}(\gamma_{\mathbf{rw}})$	$\mathbf{C_N}(\gamma_{\mathbf{rw}})$
0	-0.74	0	0
10	-0.86	0.14	0.04
20	-1.1	0.3	0.05
30	-0.88	0.48	0.062
40	-0.51	0.515	0.061
50	-0.19	0.525	0.057
60	0	0.53	0.03
70	0.16	0.525	0.001
80	0.51	0.515	-0.012
90	0.88	0.48	-0.017
100	1.15	0.3	-0.011
110	0.98	0.14	0
120	0.87	0	0
130	1.15	0.3	-0.011
140	0.98	0.14	0
150	0.87	0	0
160	1.15	0.3	-0.011
170	0.98	0.14	0
180	0.87	0	0

Table B.2: Wind force coefficients for CS3

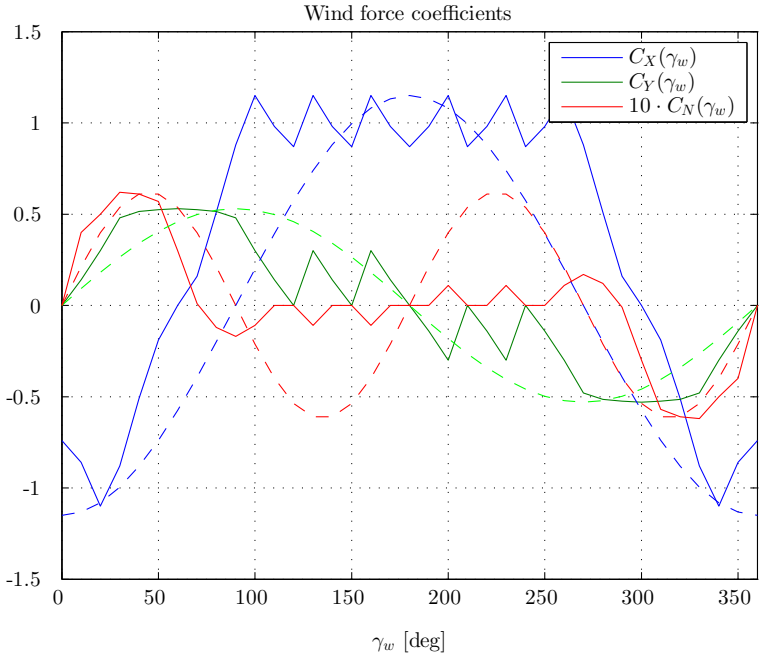

Figure B.1: Wind coefficients for CS3

B.3 Current Coefficients

γ_{rc} [deg]	$C_X(\gamma_{rc})$	$C_Y(\gamma_{rc})$	$C_N(\gamma_{rc})$
0	-0.11263	0	0
10	-0.11502	0.24276	0.074898
20	-0.127	0.51321	0.15584
30	-0.15099	0.83736	0.2257
40	-0.17735	1.1885	0.28479
50	-0.17494	1.5409	0.28479
60	-0.14618	1.837	0.18271
70	-0.10784	2.0259	0.15578
80	-0.062313	2.1332	0.064411
90	-0.016773	2.1875	-0.032204
100	0.038345	2.134	-0.15054
110	0.088673	2.0014	-0.25802
120	0.1342	1.7821	-0.35465
130	0.17494	1.4849	-0.43515
140	0.19891	1.1615	-0.45126
150	0.19891	0.86386	-0.382
160	0.18693	0.56725	-0.28479
170	0.16776	0.29712	-0.17189
180	0.14379	0	0

Table B.3: Current force coefficients for CS3

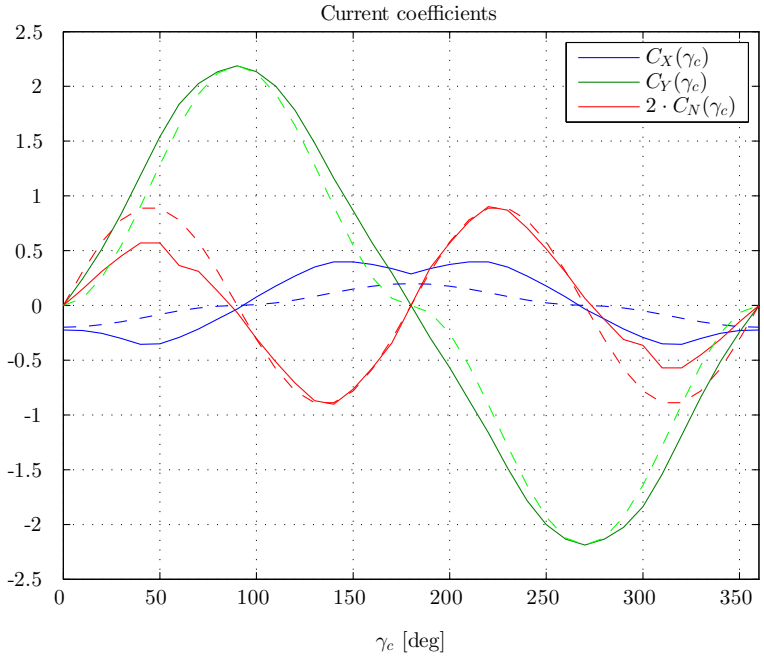

Figure B.2: Current coefficients for CS3

B.4 Motion RAOs (full scale)

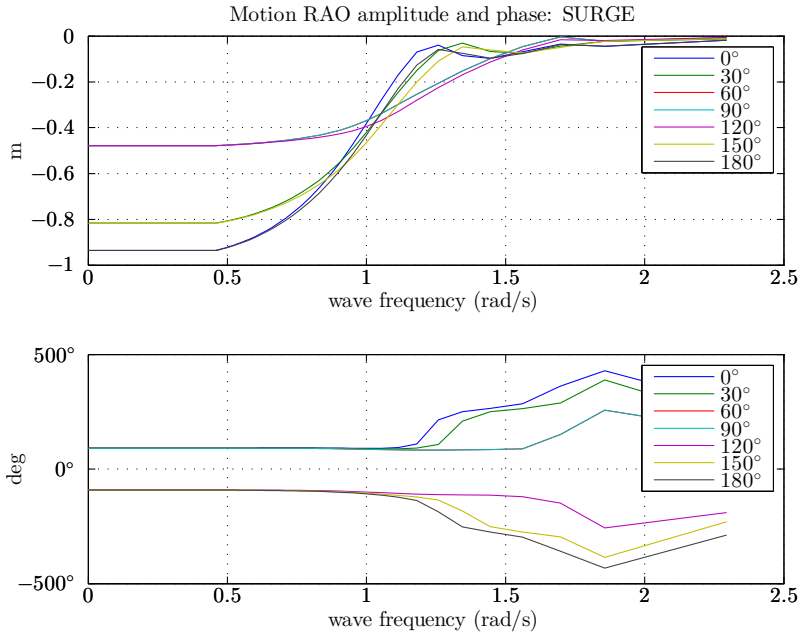

Figure B.3: Surge RAO

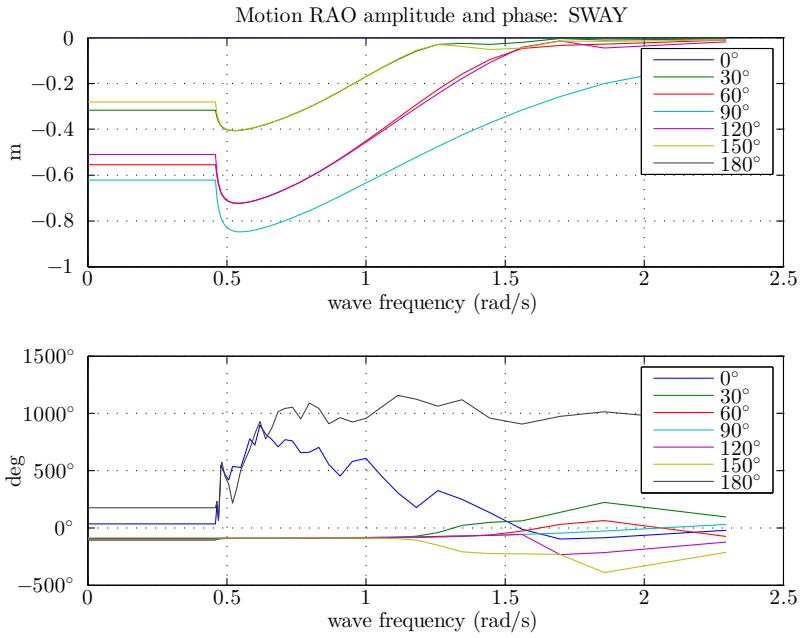

Figure B.4: Sway RAO

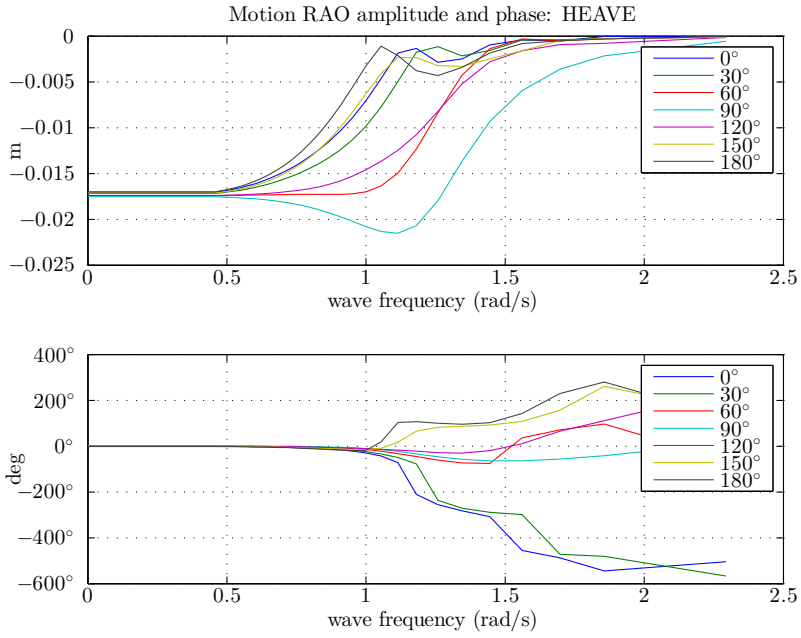

Figure B.5: Heave RAO

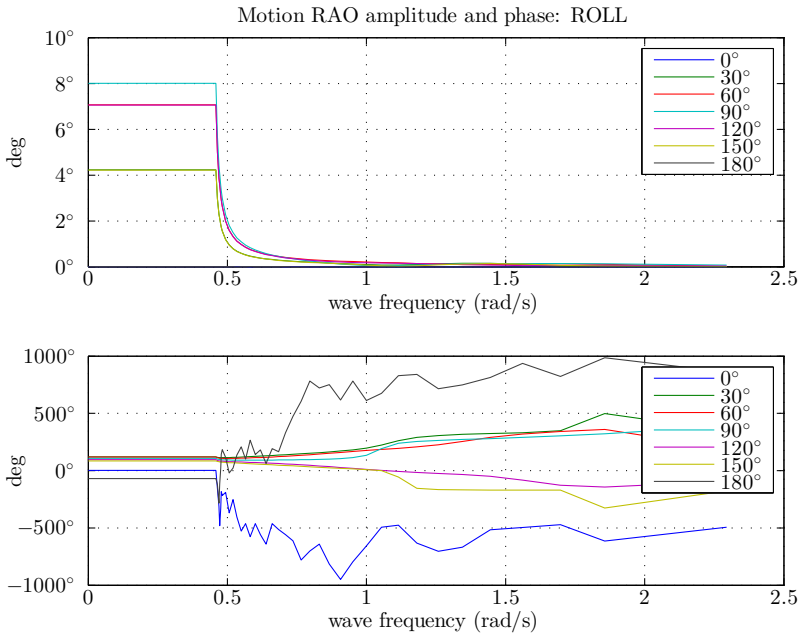

Figure B.6: Roll RAO

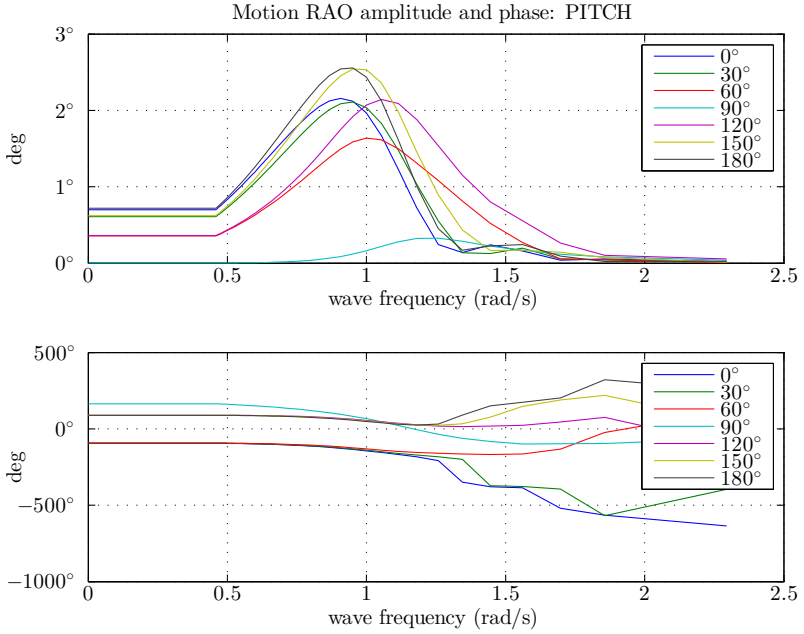

Figure B.7: Pitch RAO

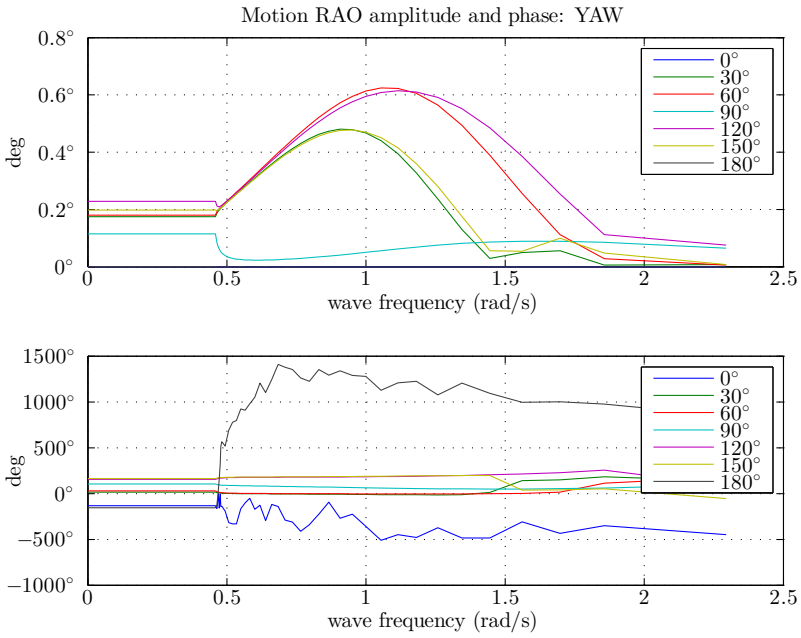

Figure B.8: Yaw RAO

Appendix C

Plots

C.1 Observer Performance

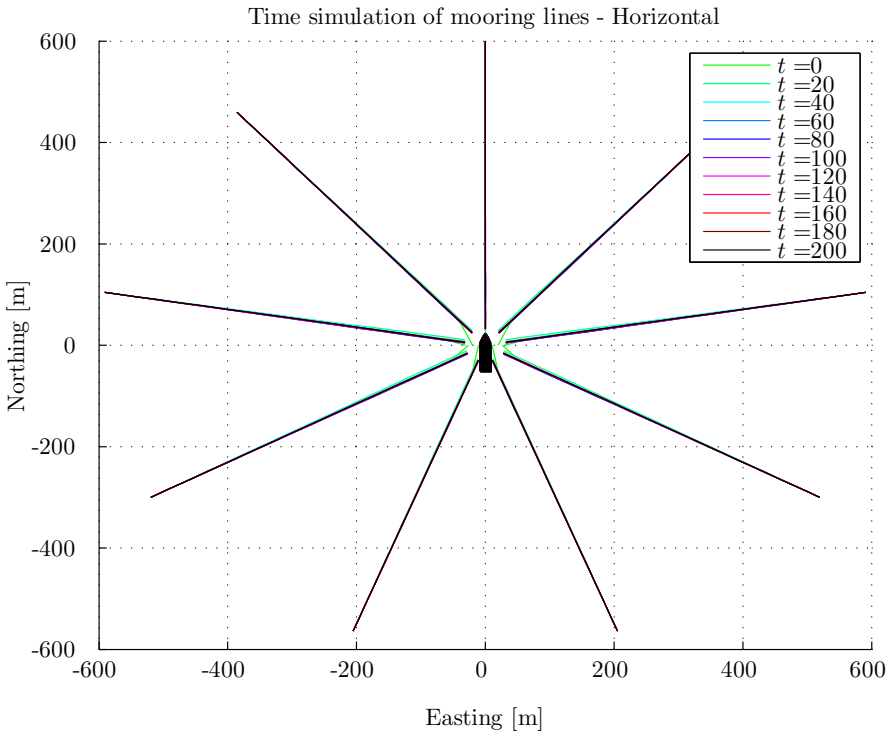

Figure C.1: Time simulation of mooring line 4 and 9

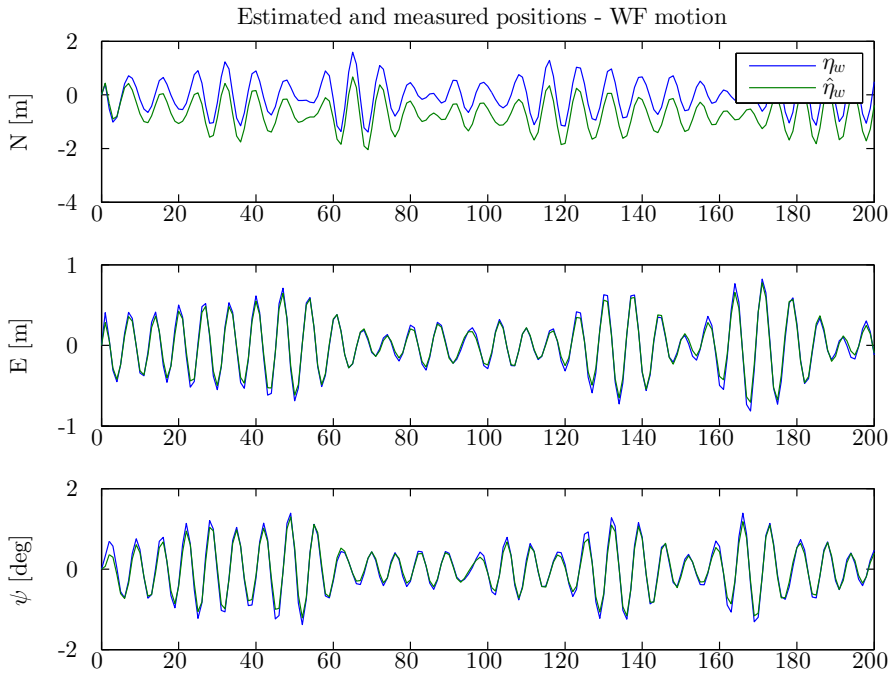
Estimated and measured positions - WF motion
N [m]
E [m]
ψ [deg]
η_w
$\hat{\eta}_w$

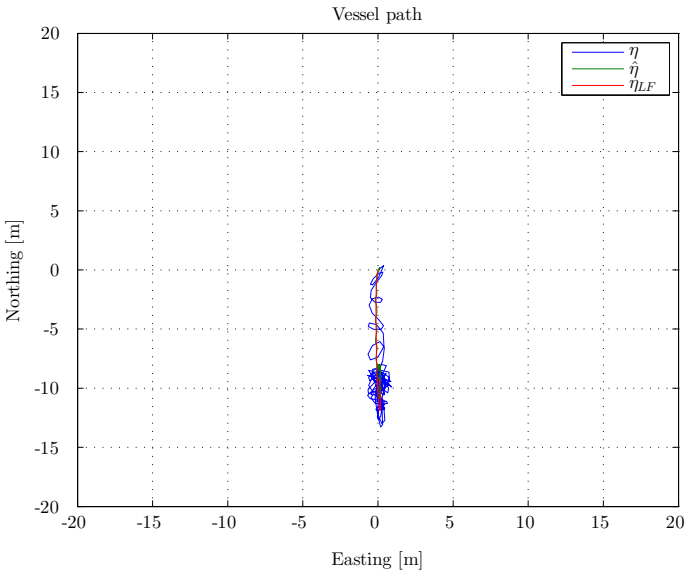
Vessel path
Northing [m]
Easting [m]
η
$\hat{\eta}$
η_{LF}

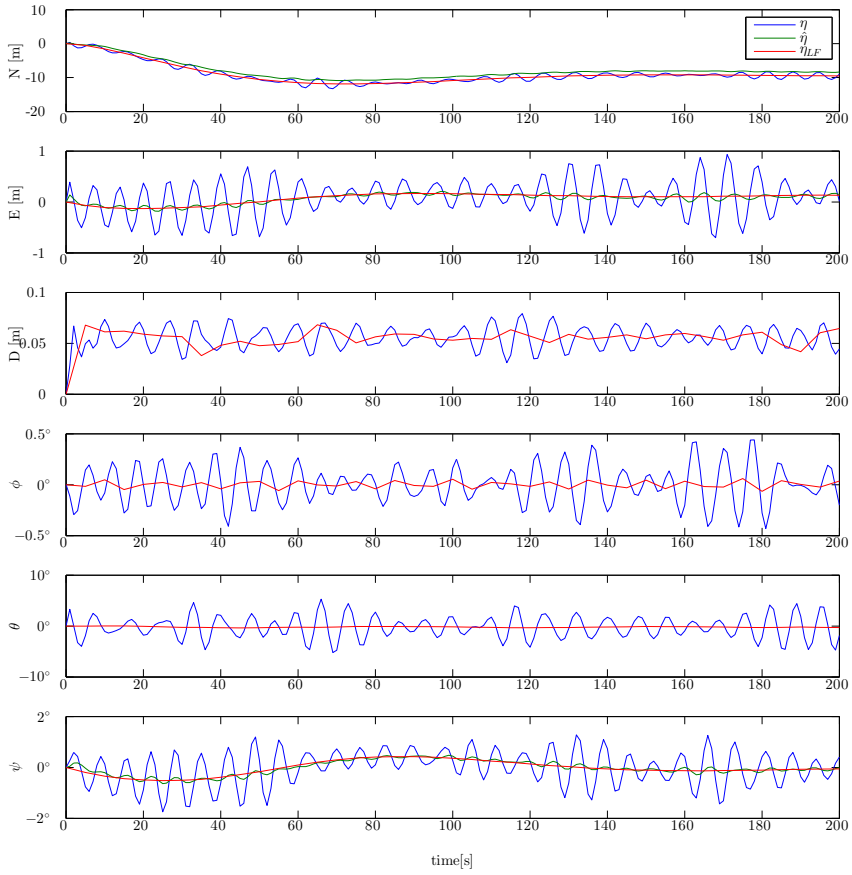
N [m]
E [m]
D [m]
ϕ
θ
ψ
η
$\hat{\eta}$
η_{LF}
time[s]

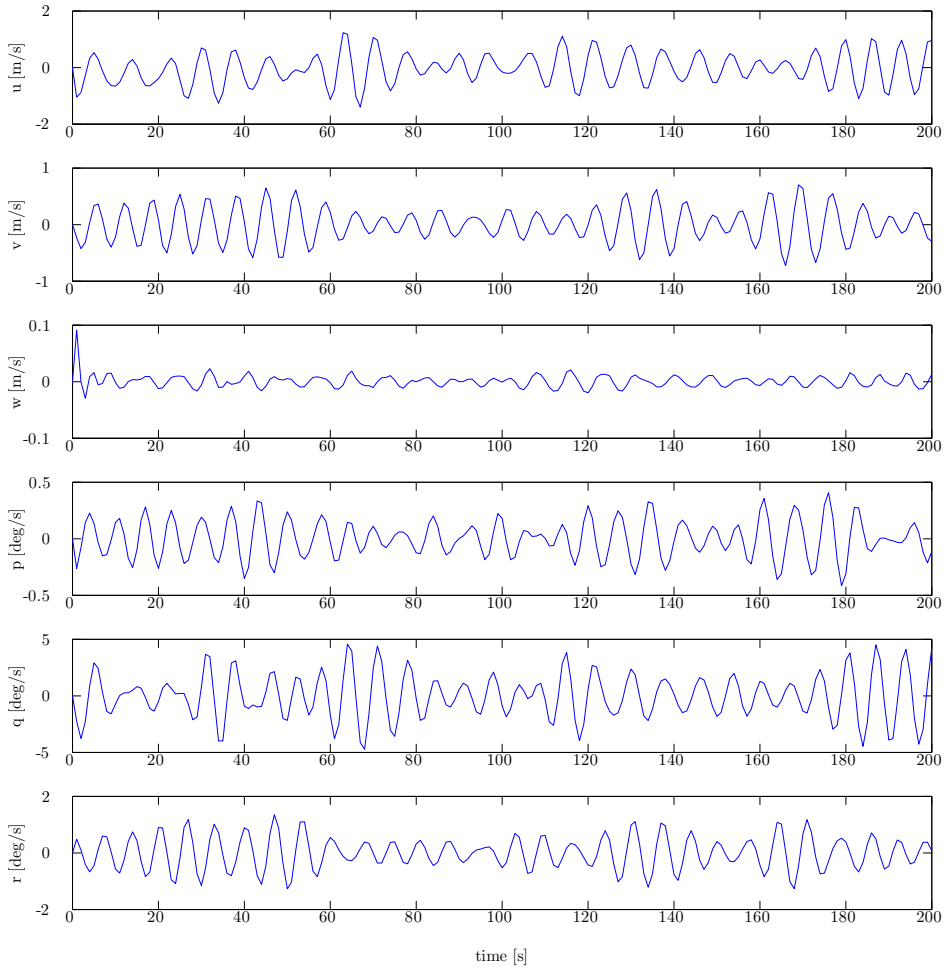
u [m/s]
v [m/s]
w [m/s]
p [deg/s]
q [deg/s]
r [deg/s]
time [s]

C.2 Control with Strong Wind and Current

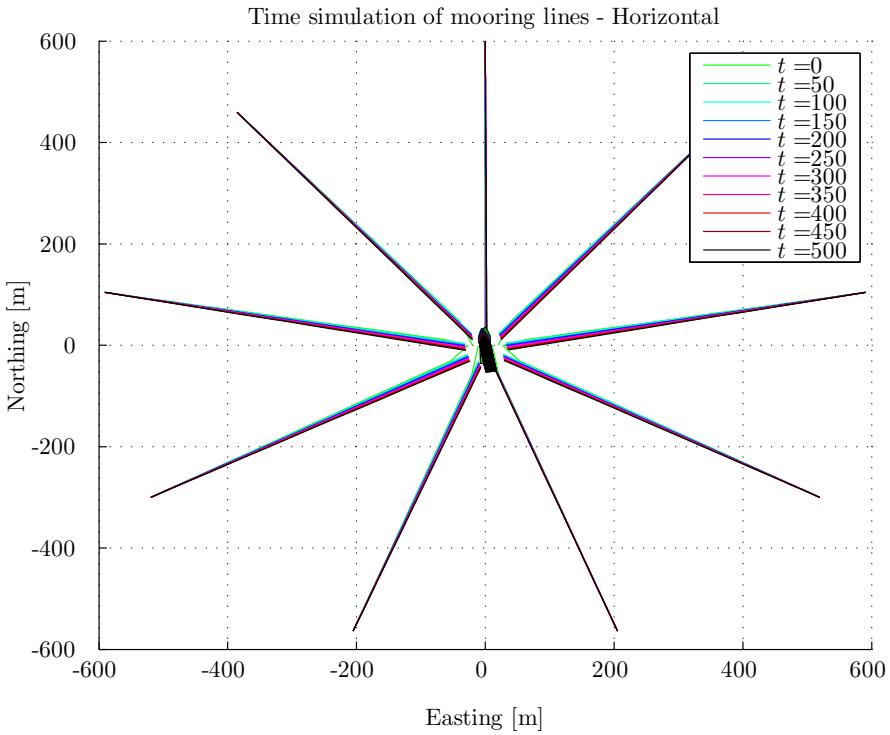

Figure C.2: Time simulation of mooring line 4 and 9

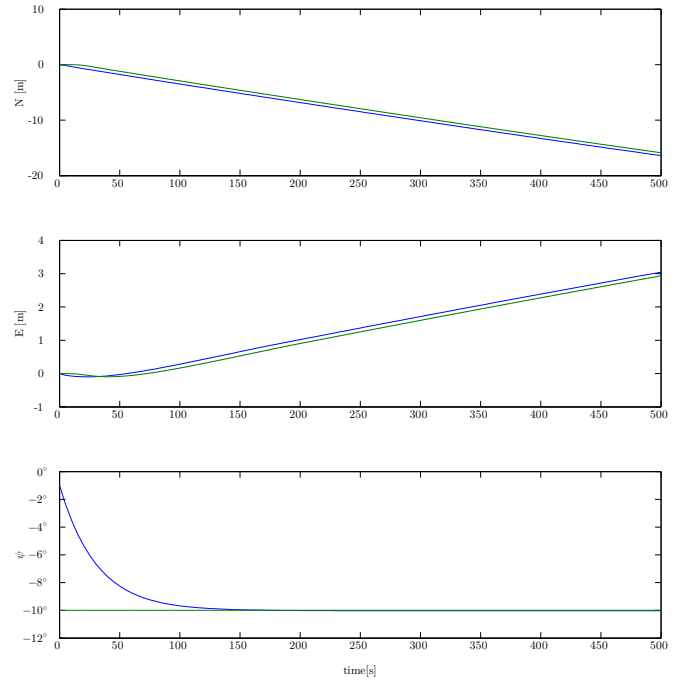
N [m]
E [m]
ψ
time[s]

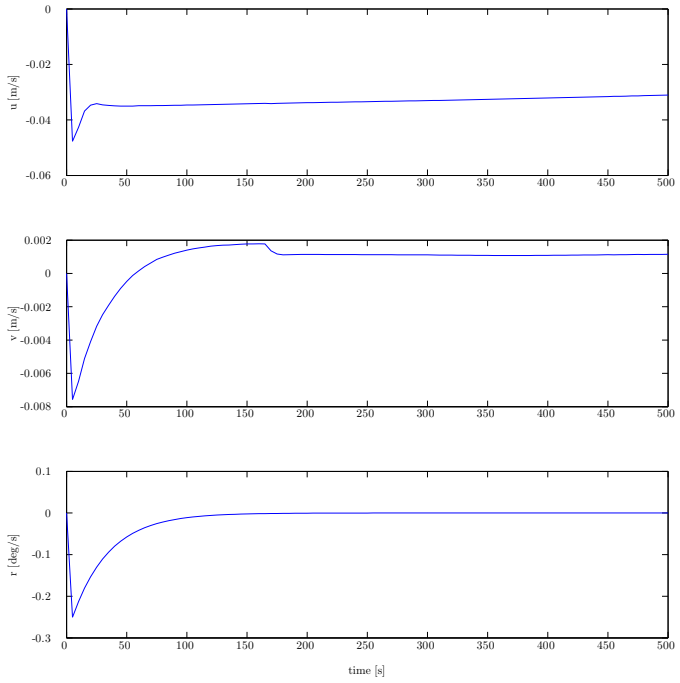
u [m/s]
v [m/s]
r [deg/s]
time [s]

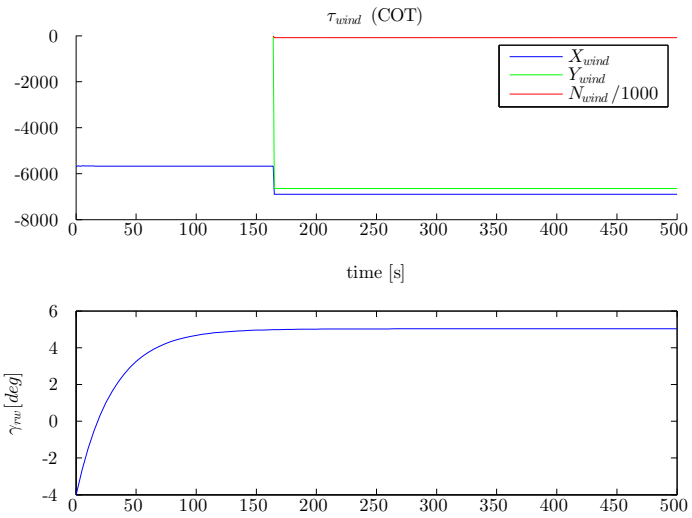
τ_{wind} (COT)
X_{wind}
Y_{wind}
$N_{wind}/1000$
time [s]
γ_{rw} [deg]

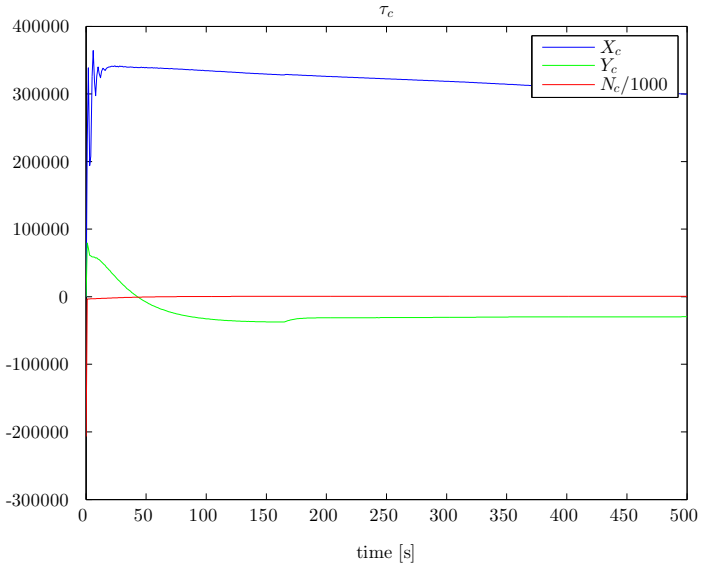
τ_c
X_c
Y_c
$N_c/1000$
time [s]

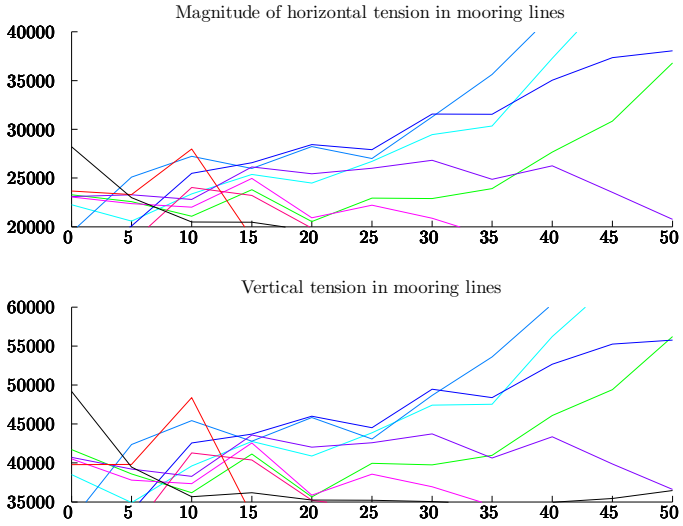

C.3 Control with Jump in Setpoint

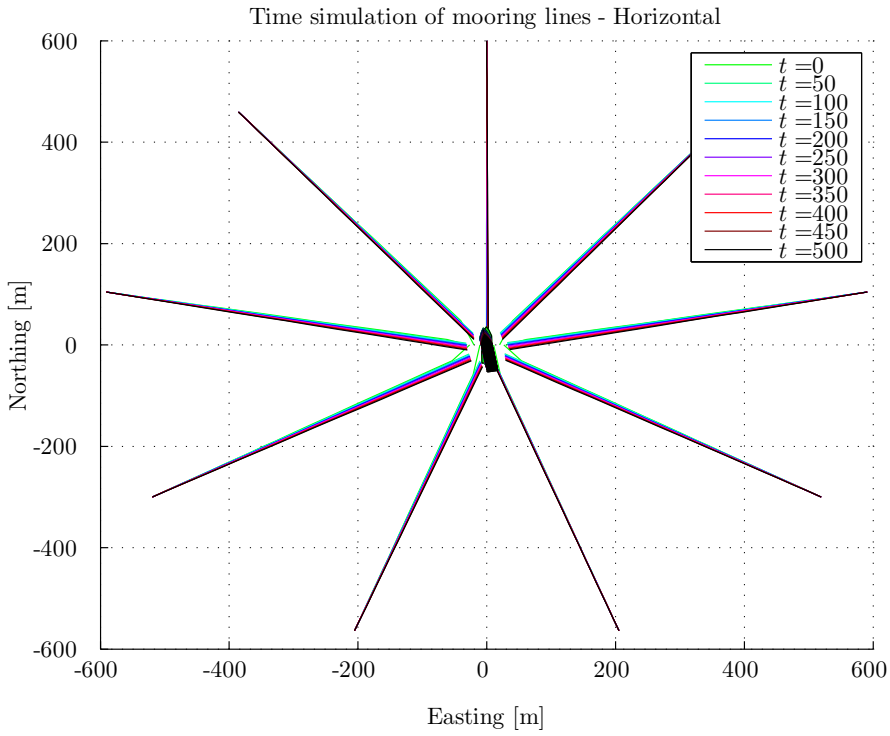

Figure C.3: Time simulation of mooring line 4 and 9

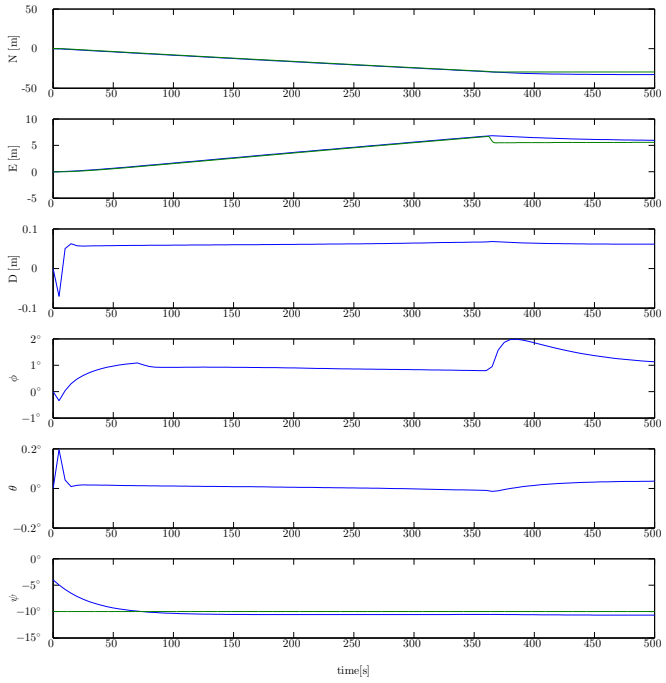
N [m]
E [m]
D [m]
ϕ
θ
ψ
time[s]

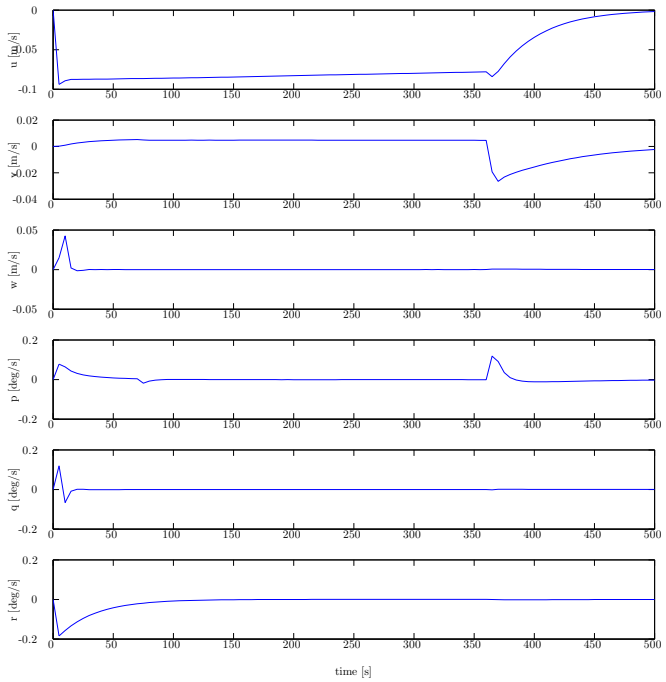
u [m/s]
v [m/s]
w [m/s]
p [deg/s]
q [deg/s]
r [deg/s]
time [s]

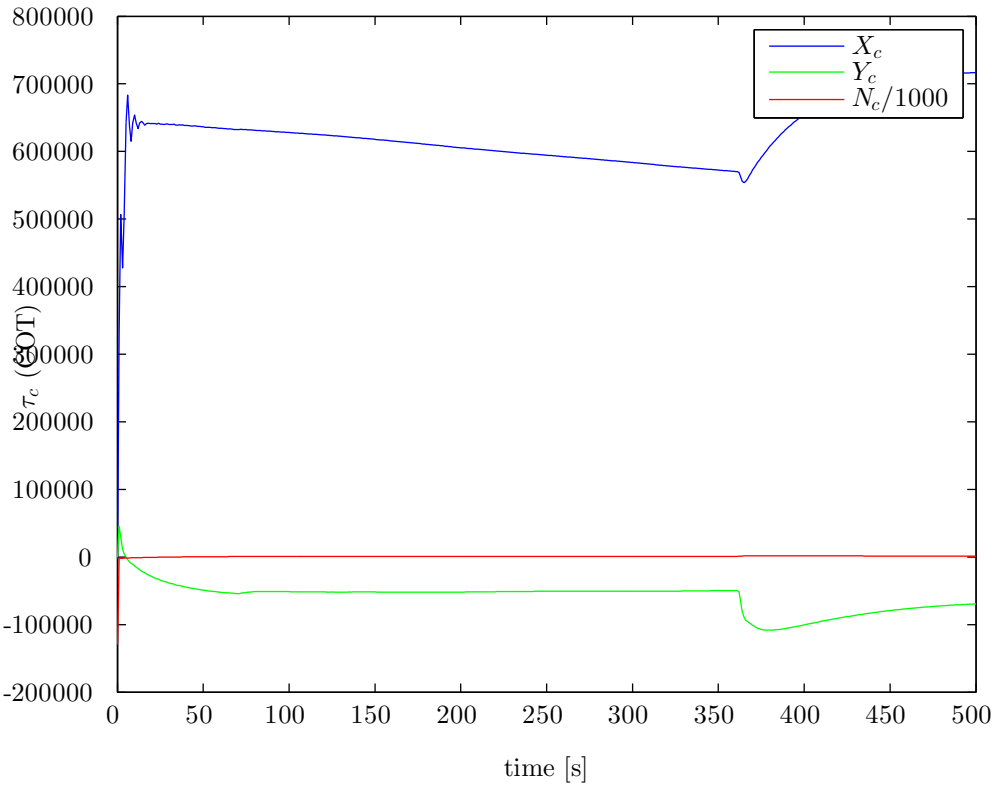
800000
700000
600000
500000
400000
300000
200000
100000
0
-100000
-200000
0
50
100
150
200
250
300
350
400
450
500
time [s]
τ_c (BOT)
X_c
Y_c
$N_c/1000$

Appendix D

Simulink diagrams

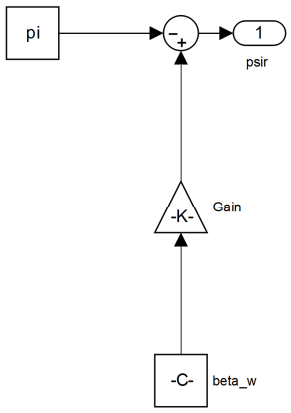

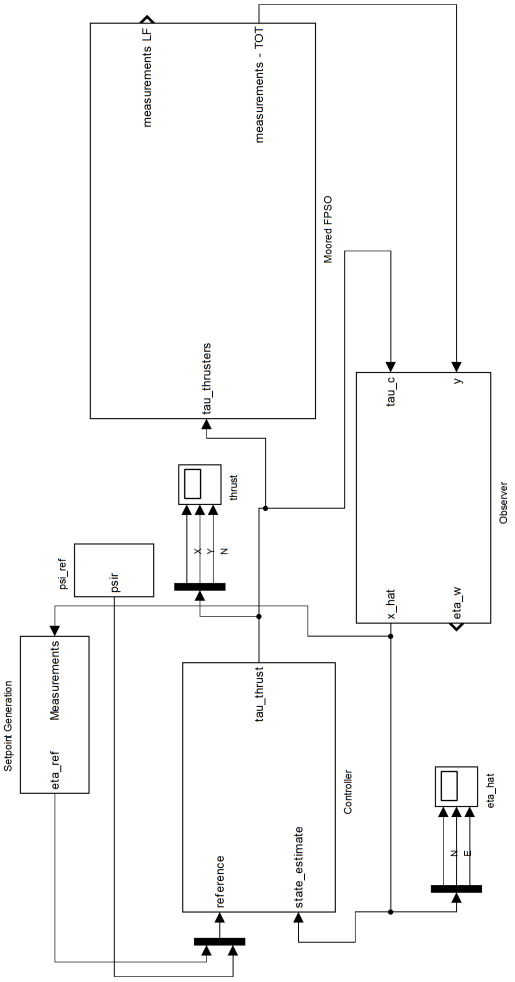
measurements LF
measurements - TOT
Moored FPSO
tau_thrusters
tau_c
y
Observer
thrust
x_hat
eta_w
psi_ref
psi
x
y
N
Setpoint Generation
Measurements
eta_ref
tau_thrust
Controller
eta_hat
N
E
reference
state_estimate

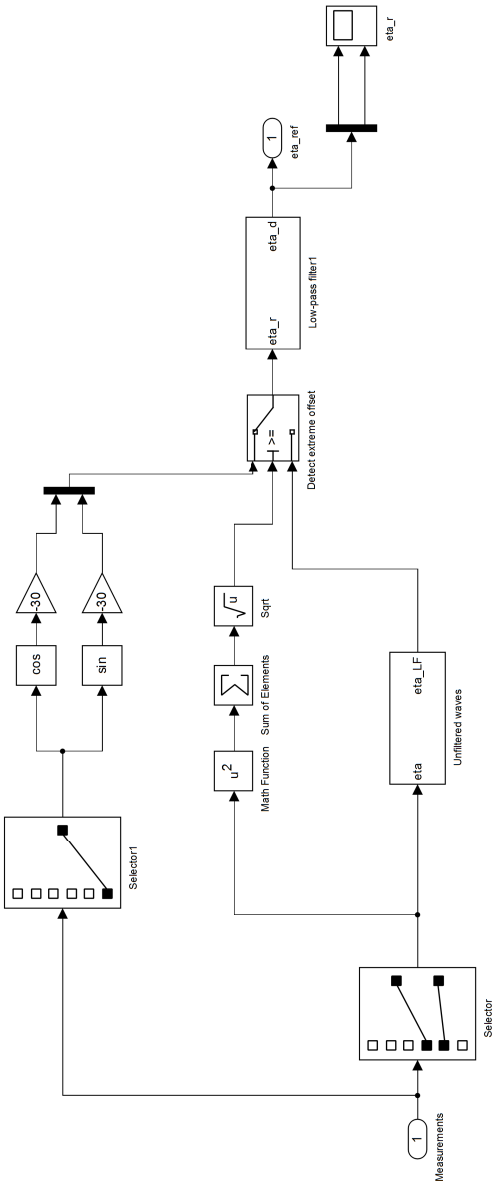
eta_r
1
eta_ref
eta_d
eta_r
Low-pass filter1
>=
Detect extreme offset
-30
-30
cos
sin
u
Sqrt
Sum of Elements
u^2
Math Function
eta_LF
eta
Unfiltered waves
Selector1
Selector
1
Measurements

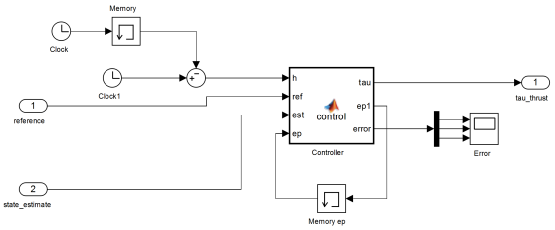
Memory
Clock
Clock1
1
reference
2
state_estimate
h
ref
est
ep
control
tau
ep1
error
Controller
1
tau_thrust
Error
Memory ep

```
function [tau,ep1,error]  = control(h, ref, est,ep)
ep0=ep;
%% PID controller

Kp=[2.0756e+05            0               0;
            0    2.0564e+05               0;
            0             0      1.3166e+09]/10;
Kd = Kp*30;

Ki = Kp*(0.1^3);

% Rotation matrix
psi = est(3);
invR = eye(3)/[ cos(psi)    -sin(psi)   0;
                sin(psi)    cos(psi)    0;
                0           0           1];

pos = [est(4) est(5) est(6)]';
ep = ref - pos;
% wrap to -pi pi
num=floor(ep(3)/(2*pi)+0.5);
ep(3)=ep(3)-num*2*pi;

nu = [est(1) est(2) est(3)]';

% Gain in body
gain = Kp*(invR*ep) - Kd*(invR*nu) - Ki*h*0.5*(invR*(ep + ep0));

tau = (gain)';
ep1=ep;
error=ep;
```

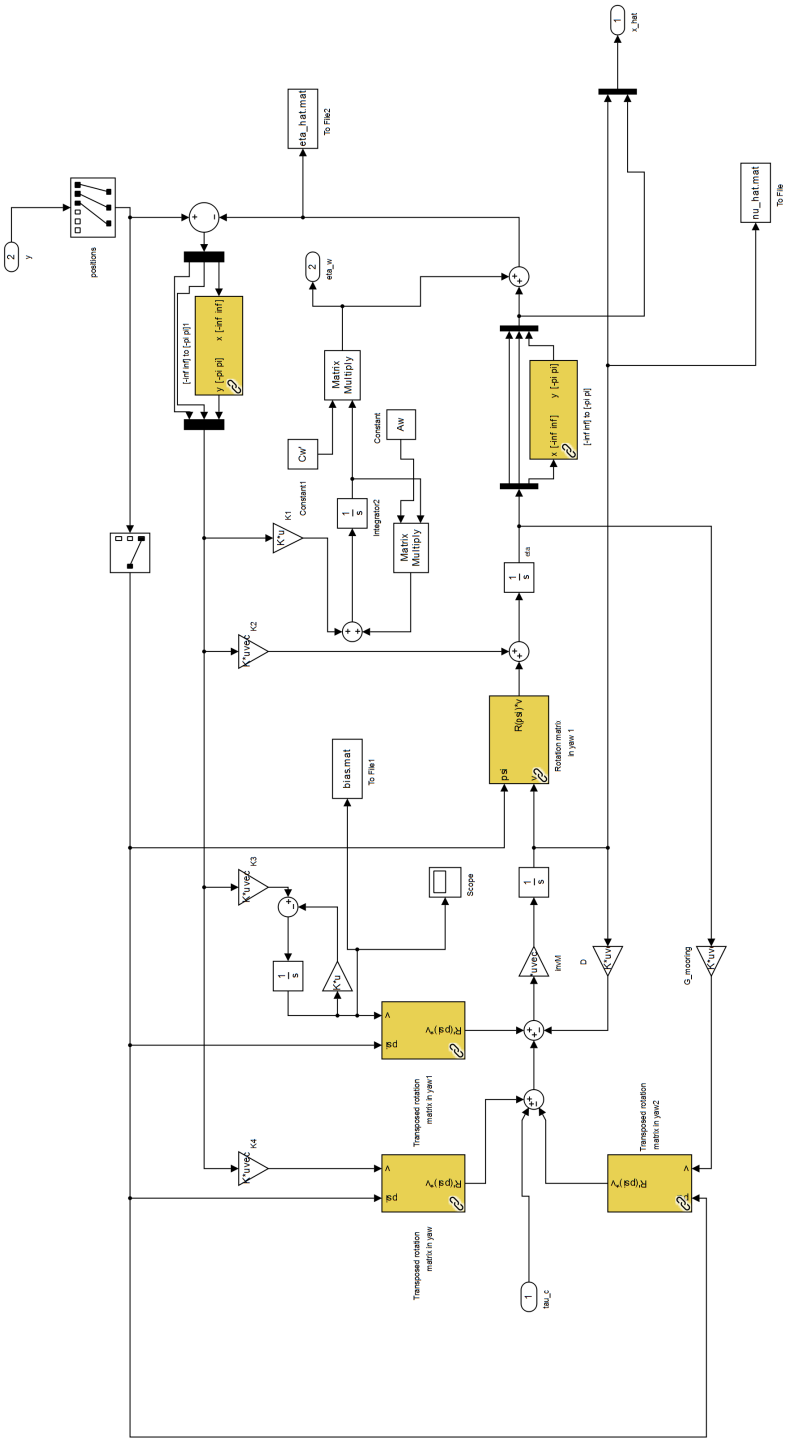
x_hat
eta_hat.mat
To File2
nu_hat.mat
To File
y
positions
eta_w
Matrix Multiply
Cw
Constant
Aw
Integrator2
Constant1
K1
K2
K3
K4
bias.mat
To File1
Rpsi'v
psi
Rotation matrix in yaw 1
Scope
invM
D
G_mooring
Transposed rotation matrix in yaw1
Transposed rotation matrix in yaw2
Transposed rotation matrix in yaw
tau_c

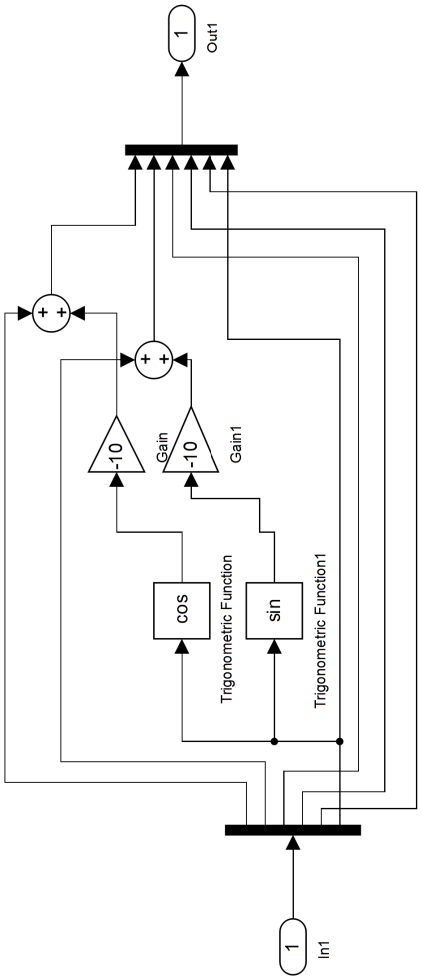
1
Out1
+ +
+ +
-10
Gain
-10
Gain1
cos
Trigonometric Function
sin
Trigonometric Function1
1
In1

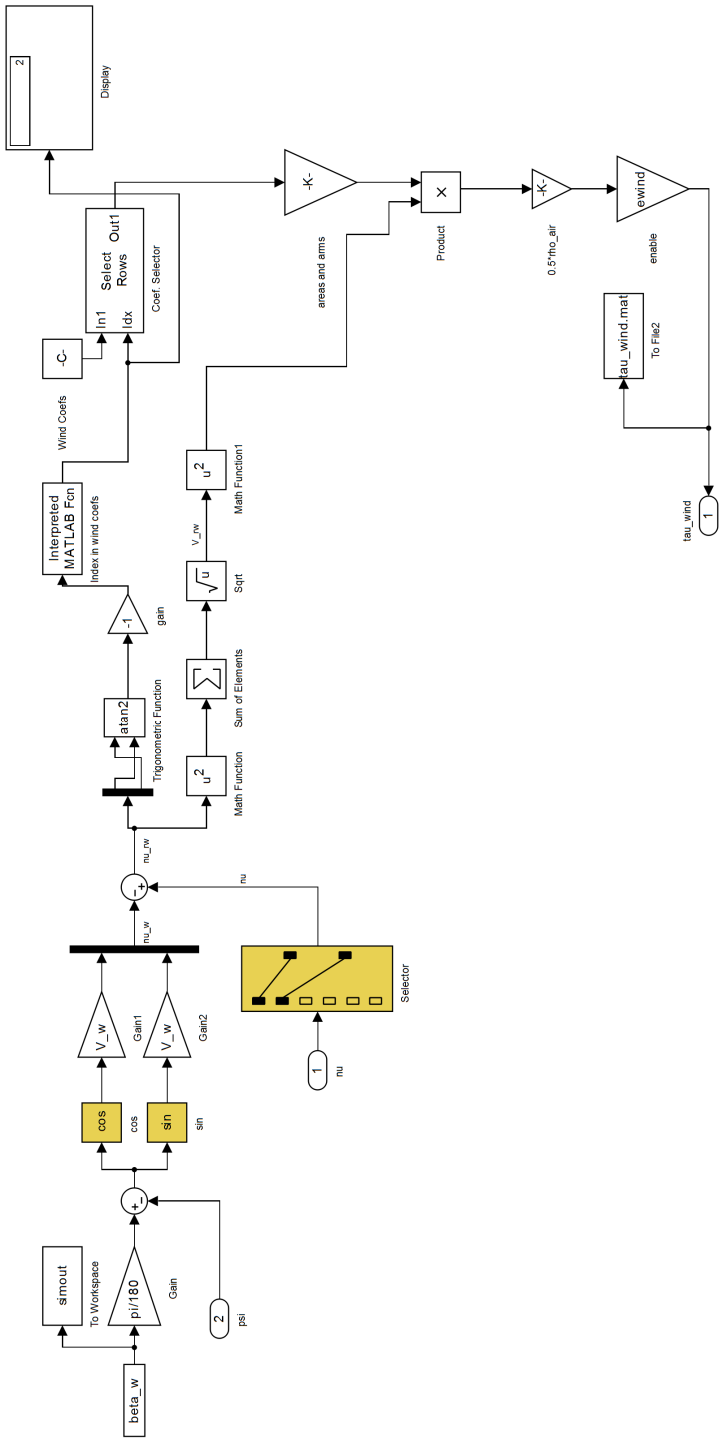
2
Display
-K-
areas and arms
Product
-K-
0.5*rho_air
ewind
enable
tau_wind.mat
To File2
tau_wind
1
Out1
Select
Rows
In1
Idx
Coef. Selector
-C-
Wind Coefs
Interpreted
MATLAB Fcn
Index in wind coefs
u^2
Math Function1
V_rw
sqrt
Sqrt
gain
-1
atan2
Trigonometric Function
Sum of Elements
u^2
Math Function
nu_rw
nu
nu_w
V_w
Gain1
V_w
Gain2
cos
cos
sin
sin
Selector
1
nu
simout
To Workspace
pi/180
Gain
2
psi
beta_w

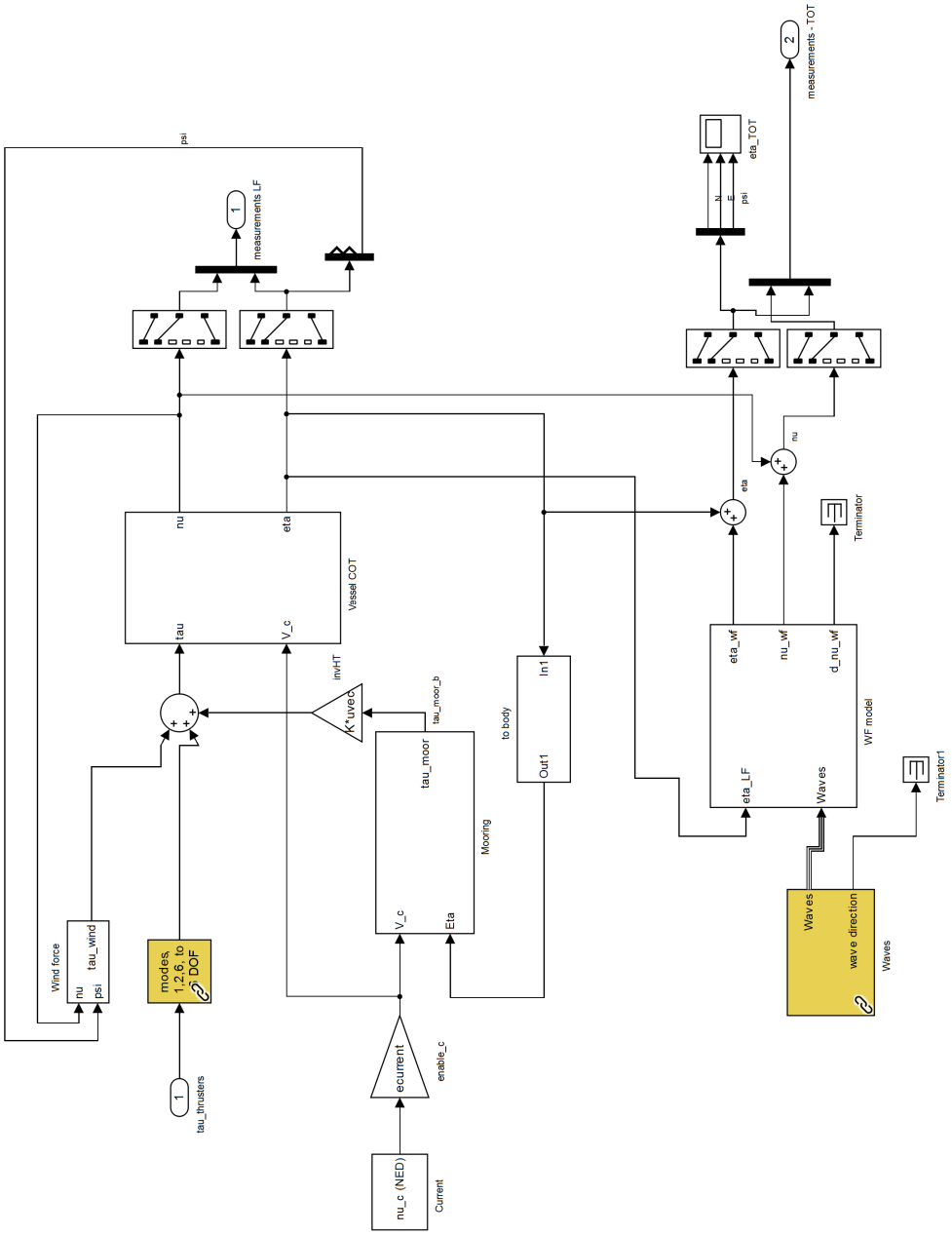
psi
1
measurements LF
2
measurements - TOT
eta_TOT
N
E
psi
nu
eta
Vessel COT
tau
V_c
eta
nu
Terminator
inv(-T
K*uvec
tau_moor_b
tau_moor
Mooring
V_c
Eta
In1
to body
Out1
eta_wf
nu_wf
d_nu_wf
WF model
eta_LF
Waves
Terminator1
Waves
wav e direction
Waves
Wind force
nu
psi
tau_wind
modes, 1:2,6, to DOF
1
tau_thrusters
ecurrent
enable_c
nu_c (NED)
Current

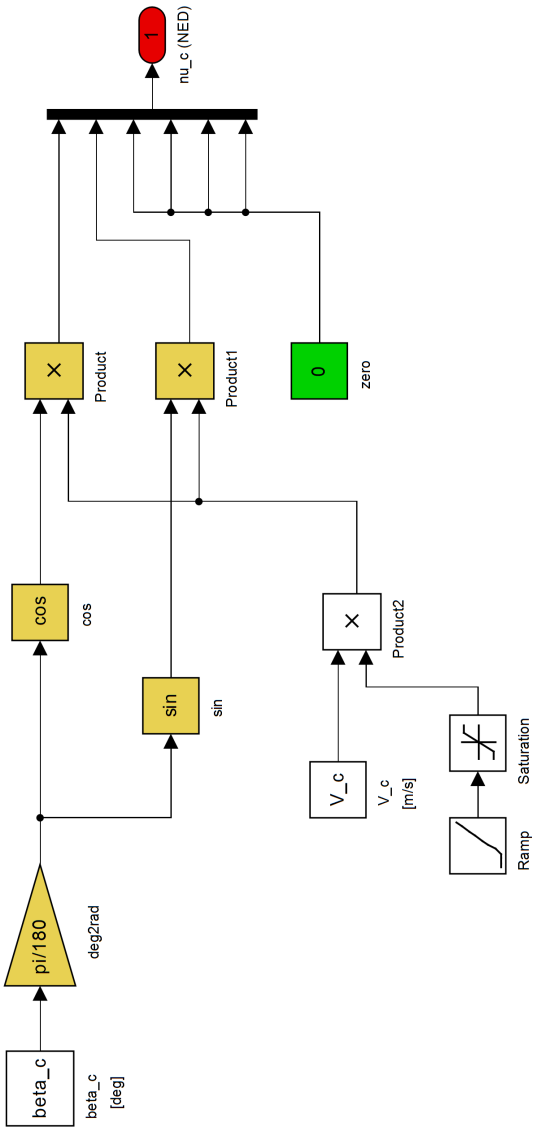
1
nu_c (NED)
Product
Product1
0
zero
cos
cos
sin
sin
Product2
V_c
V_c
[m/s]
Saturation
Ramp
pi/180
deg2rad
beta_c
beta_c
[deg]

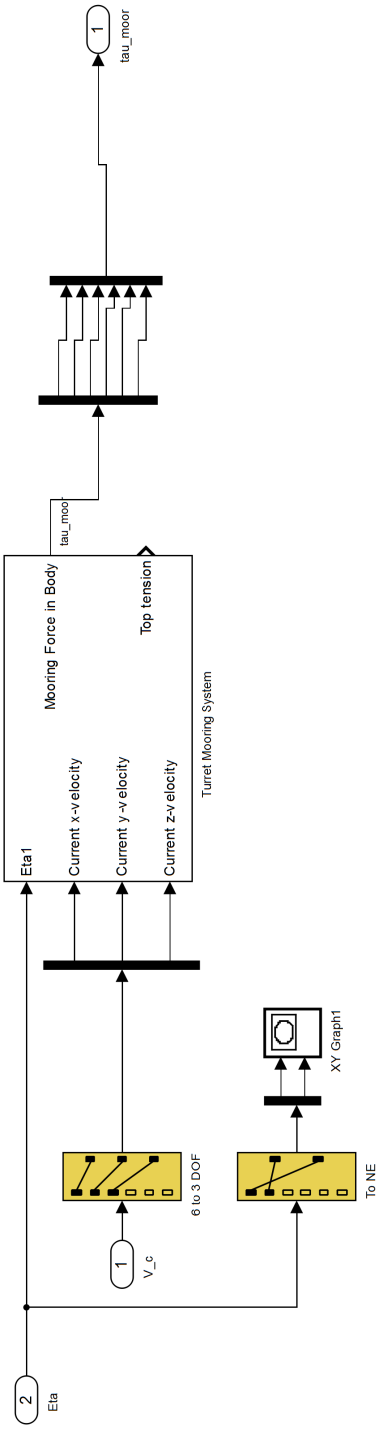
1
tau_moor
tau_moor
Mooring Force in Body
Top tension
Turret Mooring System
Eta1
Current x-v elocity
Current y-v elocity
Current z-v elocity
XY Graph1
6 to 3 DOF
To NE
1
V_c
2
Eta

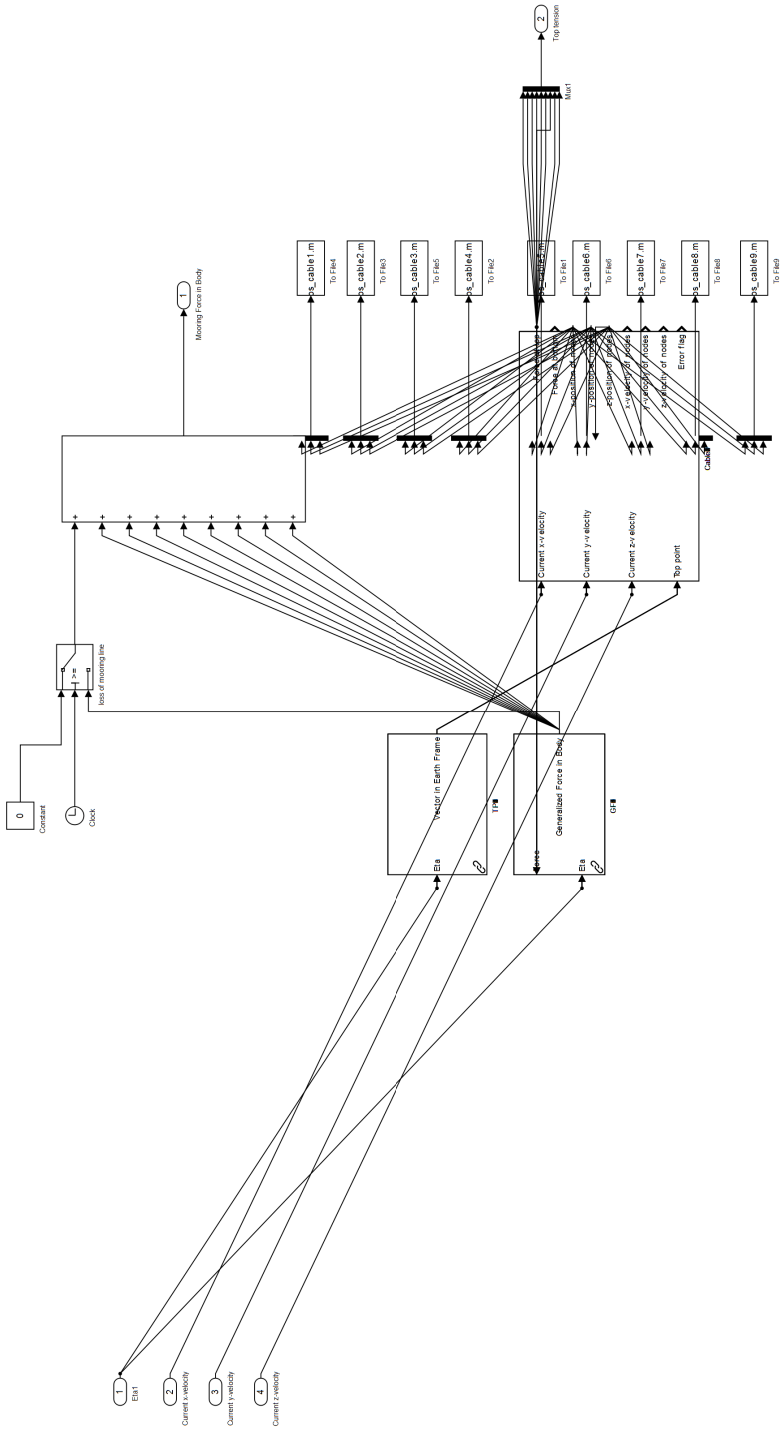
2
Top tension
Mux1
ps_cable1.m
To File4
ps_cable2.m
To File3
ps_cable3.m
To File5
ps_cable4.m
To File2
ps_cable5.m
To File1
ps_cable6.m
To File6
ps_cable7.m
To File7
ps_cable8.m
To File8
ps_cable9.m
To File9
1
Mooring Force in Body
Current x-v elocity
Current y-v elocity
Current z-v elocity
Top point
Cable9
loss of mooring line
>=
0
Constant
Clock
Vector in Earth Frame
Eta
Tau
Generalized Force in Body
Eta
Tau
1
Eta1
2
Current x-velocity
3
Current y-velocity
4
Current z-velocity

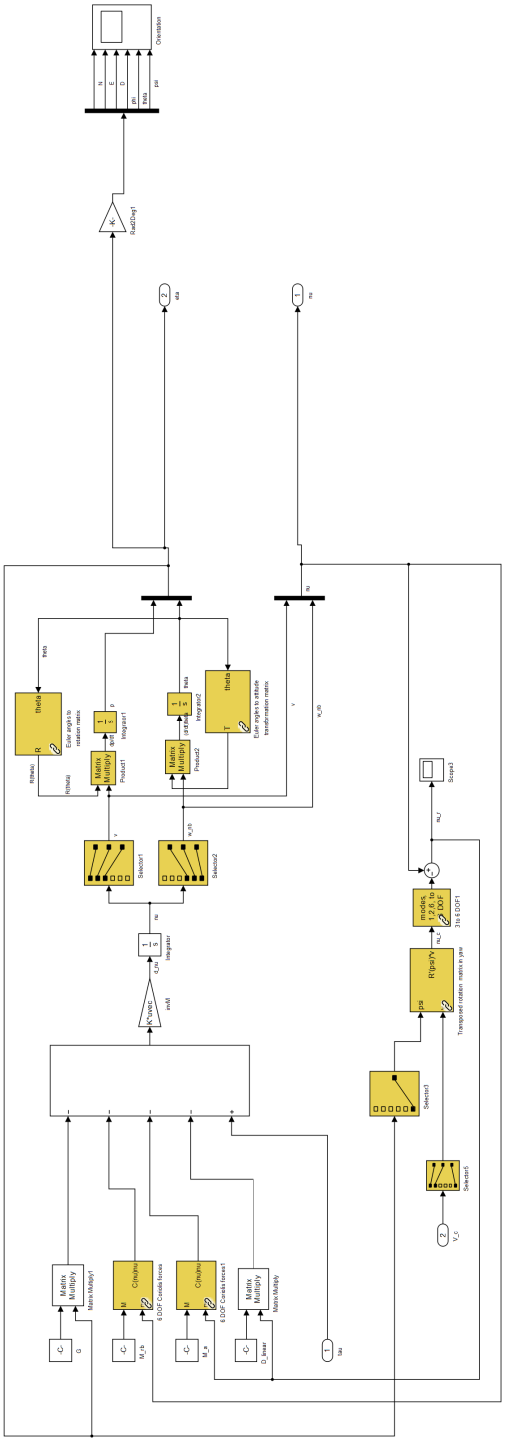
Orientation
N
E
D
phi
theta
psi
Rad2Deg1
2
eta
1
nu
theta
thetaIb
R
Euler angles to rotation matrix
Matrix Multiply
Product1
1/s
Integrator1
dphi
p
Integrator2
Product2
T
Euler angles to attitude transformation matrix
r
K_qb
Selector1
Selector2
nu
1/s
Integrator
v_dot
K*u(n)
eye(6)
Matrix Multiply
Matrix Multiply1
-C-
0
C(nu1b)
M
6 DOF Coriolis forces
M_rb
C(nu2b)
6 DOF Coriolis forces1
M_a
Matrix Multiply
Matrix Multiply2
D_linear
tau
Selector3
R'(psi)*v
Transposed rotation matrix in psi
Selector5
2
V_c
RAO
Scope3
+
+
modes, 1 to 6 DOF
1to 6 DOF1

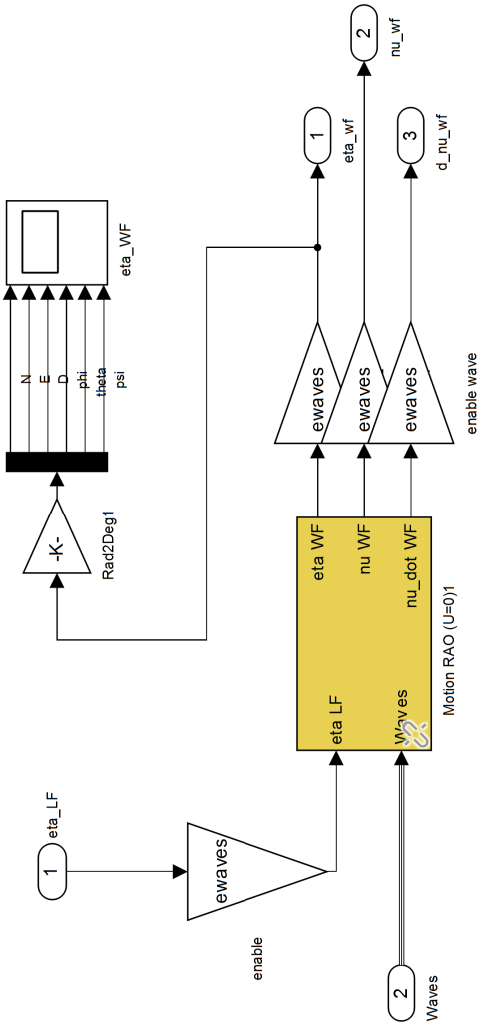
2
nu_wf
1
eta_wf
3
d_nu_wf
eta_WF
N
E
D
phi
theta
psi
-K-
Rad2Deg1
ewaves
ewaves
ewaves
enable wave
eta WF
nu WF
nu_dot WF
eta LF
Waves
Motion RAO (U=0)1
1
eta_LF
ewaves
enable
2
Waves